Chemical Engineering Journal

Braided Suture-Reinforced Fibrous Yarn Bundles as a Scaffold for Tendon Tissue Engineering in Extensor Digitorum Tendon Repair

--Manuscript Draft--

Manuscript Number:	CEJ-D-22-21954
Article Type:	Research Paper
Section/Category:	Novel Materials for Energy and Advanced Applications
Keywords:	Electrospinning; scaffold; yarn; tissue engineering; dynamic culture; basic fibroblast growth factor
Corresponding Author:	Jyh-Ping Chen Chang Gung University Taoyuan, Taiwan
First Author:	K.T. Shalumon
Order of Authors:	K.T. Shalumon
	Han-Tsung Liao
	Wei-Hao Lin
	Mini P.A.
	Jyh-Ping Chen
Abstract:	In this study, we intend to develop an effective tendon tissue engineering scaffold that can provide mechanical stability and tendon regeneration ability. Using a novel electrospinning process, a biodegradable suture was continuously covered with aligned polycaprolactone fibers in core/sheath structure to produce a single yarn. The single yarn was braided together to fabricate a multi yarn (MY) scaffold, which can be surface modified with oxygen plasma and conjugated with heparin. The fibroblast growth factor 2 (FGF2) was bound to MY through bioaffinity between heparin and FGF2 to generate a functional scaffold (MY-FGF2) suitable for extensor digitorum tendon (EDT) repair. The physico-chemical properties of the scaffolds were characterized throughout the modification steps using microscopy, spectroscopy and mechanical testing. In vitro static culture using rabbit tendon-derived fibroblasts (rTFs) indicates combined effects of FGF2 and fiber alignment can enhance cell proliferation and extracellular matrix synthesis rates, as well as fasten tendon maturation. The cytoskeleton staining further endorses aligned morphology of fibers direct cell growth and collagen fiber deposition along the fiber axial direction, mimicking native tendon features. The dynamic culture in a bioreactor under uniaxial cyclic tensile loading authenticates 5% mechanical stimulation can further increase cell proliferation and tenogenic differentiation rates compared to static culture. After mechanical stimulation for 7 days in vitro, the MY-FGF2/rTFs construct was used for repair of EDT defects in rabbits. The retrieved MY-FGF2/rTFs sample 6-week post-implantation shows superior mechanical properties and tendon regeneration abilities over acellular MY-FGF2. Taken together, we demonstrate a combinatory approach with MY-FGF2 where chemical and physical cues provided by FGF2, fiber alignment and dynamic stimulation contribute to tendon regeneration with a specific focus on EDT repair.

CHANG GUNG UNIVERSITY

September 16, 2022

Editor
Chemical Engineering Journal

Dear Editor:

We would like to submit a manuscript for consideration to be published in **Chemical Engineering Journal**.

Manuscript title: Braided Suture-Reinforced Fibrous Yarn Bundles as a Scaffold for Tendon Tissue Engineering in Extensor Digitorum Tendon Repair

Name of corresponding author: Jyh-Ping Chen

Name of all other authors: K.T. Shalumon, Han-Tsung Liao, Wei-Hao Lin, Mini P.A.

Type of Manuscript: Original paper

Significance: In this work, a novel electrospinning process was used to cover a biodegradable suture core with aligned polycaprolactone fiber sheath to produce a single yarn. Three single yarns were braided to fabricate a mechanical stable multi yarn (MY) scaffold for tendon tissue engineering. To introduce biochemical cues, MY was surfaced modified with heparin for binding with basic fibroblast growth factor (FGF2). In vitro studies using MY-FGF2 and rabbit tendon fibroblasts (rTFs) show enhanced cell proliferation and ECM synthesis rate as well as accelerated tendon maturation. Dynamic culture of MY-FGF2/rTFs under 5% cyclic tensile strains further increases cell proliferation and tenogenic differentiation rate. A dynamically cultured MY-FGF2/rTFs construct can repair EDT defect in rabbits with superior tendon regeneration abilities.

List of keywords: Electrospinning; scaffold; yarn; tissue engineering; dynamic culture; basic fibroblast growth factor

Authors' statements: The author has consulted the Guide for Authors in preparing the submitted manuscript and prepared the manuscript in compliance with the Ethics in Publishing Policy as described in the Guide for Authors. All authors have seen and approved the submission of the manuscript to the journal. The manuscript has not been published previously by any of the authors and/or is not under consideration for publication in another journal.

Names and addresses of recommend reviewers:

1. Dr. Helmut Thissen
Molecular Science
CSIRO
Australia
E-mail: helmut.thissen@csiro.au

2. Dr. Wenguo Cui
School of Medicine
Shanghai Jiao Tong University
China
wgcui80@hotmail.com

3. Dr. R. Jayakumar
Amrita Center for Nanosciences and Molecular Medicine
Amrita Institute of Medical Sciences and Research Centre
India
E-mail: rjayakumar@aims.amrita.edu

4. Dr. Tasuku Nakajima
Faculty of Advanced Life Science
Hokkaido University
Japan.
E-mail: tasuku@sci.hokudai.ac.jp

5. Dr. Cato T. Laurencin
Materials Science and Engineering
University of Connecticut
laurencin@uchc.edu

We hope that you will consider this manuscript for publication, and we are at your full disposal for any modifications suggested during the review process.

Sincerely yours,

Jyh-Ping Chen, PhD
Professor
Department of Chemical and Materials Engineering
Chang Gung University
Taoyuan, Taiwan, ROC

Names and addresses of recommend reviewers:

1. Dr. Helmut Thissen
Molecular Science
CSIRO
Australia
E-mail: helmut.thissen@csiro.au

2. Dr. Wenguo Cui
School of Medicine
Shanghai Jiao Tong University
China
wgcui80@hotmail.com

3. Dr. R. Jayakumar
Amrita Center for Nanosciences and Molecular Medicine
Amrita Institute of Medical Sciences and Research Centre
India
E-mail: rjayakumar@aims.amrita.edu

4. Dr. Tasuku Nakajima
Faculty of Advanced Life Science
Hokkaido University
Japan.
E-mail: tasuku@sci.hokudai.ac.jp

5. Dr. Cato T. Laurencin
Materials Science and Engineering
University of Connecticut
laurencin@uchc.edu

Graphical Abstract

TOC Graphic

Braided Suture-reinforced Fibrous Yarn Bundles as a Scaffold for Tendon Tissue Engineering in Extensor Digitorum Tendon Repair

K.T. Shalumon, Han- Tsung Liao, Wei-Hao Lin, Mini P.A., Jyh-Ping Chen

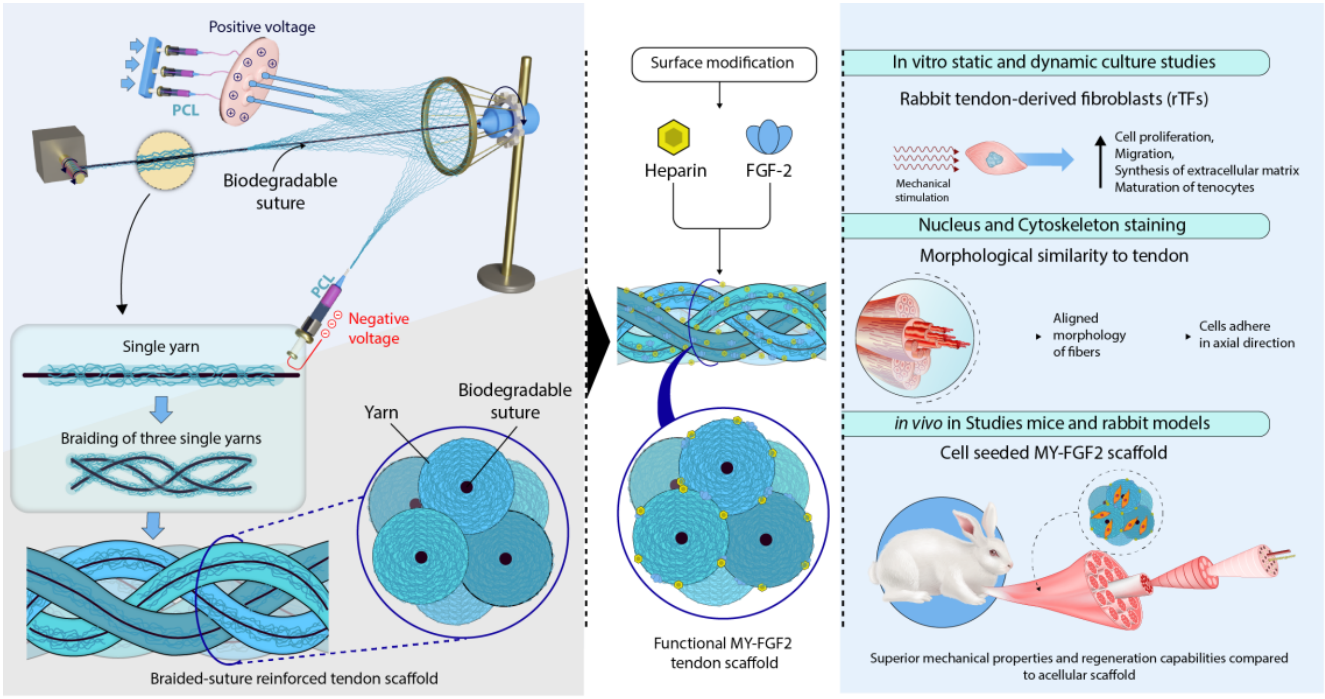

rTFs seeded/mechanically stimulated MY-FGF2 scaffold is a promising candidate for tendon regeneration, with a specific focus on EDT repair

Highlights

1. A novel electrospinning process can cover a biodegradable suture core with aligned polycaprolactone fiber sheath.
2. Three yarns were braided to fabricate a mechanical stable multi yarn (MY) scaffold for tendon regeneration.
3. To introduce biochemical cues, MY was surfaced modified with heparin for binding with FGF2 (MY-FGF2).
4. In vitro study with MY-FGF2/rTFs shows enhanced cell proliferation, ECM synthesis and accelerated tendon maturation rate.
5. Dynamic culture of MY-FGF2/rTFs under 5% cyclic tensile strains further increases cell proliferation and tenogenic differentiation rate.
6. A dynamically cultured MY-FGF2/rTFs construct can repair EDT defect in rabbits with superior tendon regeneration abilities.

Braided Suture-Reinforced Fibrous Yarn Bundles as a Scaffold for Tendon Tissue Engineering in Extensor Digitorum Tendon Repair

K.T. Shalumon[1,2†], Han- Tsung Liao[3†], Wei-Hao Lin[1], Mini P.A.[4], Jyh-Ping Chen[1,3,5,6,7*]

[1]Department of Chemical and Materials Engineering, Chang Gung University, Kwei-San, Taoyuan 33302, Taiwan

[2]Department of Chemistry, Sacred Heart College, MG University, Kochi 682013, India

[3]Department of Plastic and Reconstructive Surgery and Craniofacial Research Center, Chang Gung Memorial Hospital at Linkou, Chang Gung University College of Medicine, Kwei-San, Taoyuan 33305, Taiwan

[4]Department of Physics, St. Michael's College, Cherthala, University of Kerala, Kerala 688539, India

[5]Department of Neurosurgery, Chang Gung Memorial Hospital at Linkou, Kwei-San, Taoyuan 33305, Taiwan

[6]Research Center for Food and Cosmetic Safety, College of Human Ecology, Chang Gung University of Science and Technology, Kwei-San, Taoyuan 33302, Taiwan

[7]Department of Materials Engineering, Ming Chi University of Technology, Tai-Shan, New Taipei City 24301, Taiwan

† K.T. Shalumon and Han-Tsung Liao contributed equally to this work

*Corresponding author

Tel: +886-3-2118800

E-mail: jpchen@mail.cgu.edu.tw

Keyword: Electrospinning; scaffold; yarn; tissue engineering; dynamic culture; basic fibroblast growth factor

Abstract In this study, we intend to develop an effective tendon tissue engineering scaffold that can provide mechanical stability and tendon regeneration ability. Using a novel electrospinning process, a biodegradable suture was continuously covered with aligned polycaprolactone fibers in core/sheath structure to produce a single yarn. The single yarn was braided together to fabricate a multi yarn (MY) scaffold, which can be surface modified with oxygen plasma and conjugated with heparin. The fibroblast growth factor 2 (FGF2) was bound to MY through bioaffinity between heparin and FGF2 to generate a functional scaffold (MY-FGF2) suitable for extensor digitorum tendon (EDT) repair. The physico-chemical properties of the scaffolds were characterized throughout the modification steps using microscopy, spectroscopy and mechanical testing. In vitro static culture using rabbit tendon-derived fibroblasts (rTFs) indicates combined effects of FGF2 and fiber alignment can enhance cell proliferation and extracellular matrix synthesis rates, as well as fasten tendon maturation. The cytoskeleton staining further endorses aligned morphology of fibers direct cell growth and collagen fiber deposition along the fiber axial direction, mimicking native tendon features. The dynamic culture in a bioreactor under uniaxial cyclic tensile loading authenticates 5% mechanical stimulation can further increase cell proliferation and tenogenic differentiation rates compared to static culture. After mechanical stimulation for 7 days in vitro, the MY-FGF2/rTFs construct was used for repair of EDT defects in rabbits. The retrieved MY-FGF2/rTFs sample 6-week post-implantation shows superior mechanical properties and tendon regeneration abilities over acellular MY-FGF2. Taken together, we demonstrate a combinatory approach with MY-FGF2 where chemical and physical cues provided by FGF2, fiber alignment and dynamic stimulation contribute to tendon regeneration with a specific focus on EDT repair.

1. INTRODUCTION

Tendons are fibrous soft connective tissues responsible for transmitting force and connecting muscles and bones. Its main function is to stretch like a highly flexible elastic spring that moves back and forth through elastic recovery. The mass of a tendon consists of 30% water, with the remaining dry mass consisting of 86% type I collagen, 1-5% proteoglycan, 2% elastic fibers, 0.2% inorganic ingredients, and a small amount of other types of collagen [1]. Considering the hierarchical structure of a tendon tissue, collagen fibrils (~300 nm) in tendons are composed of collagen triple helix molecules of 20 to 150 nm diameter. These collagen fibrils further form collagen fibers (20 μm), by arranging themselves

in a longitudinal manner and lead to a structure with high tensile strength. With parallel arrangement, the collagen fibers in turn are bundled by tendon endocardium (endotenon) to form fiber bundles (fascicles) with ~300 μm in size. These fiber bundles are also arranged longitudinal to provide tensile strength of the tendon [2]. Therefore, with the complex structure of tendon tissues, tendon repair has always been a problem for clinicians. In current scenario, traditional clinical reconstruction and repair of tendon tissues follow two directions, i.e. allografts or autografts. The allografts face problems like disease transmission, lack of durability and functionality, insufficient supply, as well as storage methods during transportation [3]. Considering this, auto-transplantation is widely used in a clinical setting, where tendon autograft may provide the most satisfactory long-term results without immune rejection. However, the possible necrotic behavior of the implant after transplantation could result in inferior biomechanical stability and thereby leads to failure of the graft after tendon reconstruction surgery.

Tissue engineering has been recognized as a promising strategy for tendon repair or reconstruction [4]. Various studies have been performed to understand the relevance of fibrillary microarchitecture and the functional characteristics of native tendon extracellular matrix (ECM). One of the long-term needs in tendon tissue engineering is to recover the damaged tissues with full regeneration of their biological functions. Therefore, a functional tissue engineered tendon should have good biological activity as well as suitable biomechanical properties. For this, cells seeded in a tissue engineering scaffold for tendon regeneration should retain good proliferation ability and induce phenotype maintenance or differentiate towards the tenogenic lineage during long-term culture in vitro [5]. In order to achieve this goal, a three-dimensional (3D) scaffold for tendon tissue engineering should be biodegradable, biocompatible, provide proper space for cell growth, and ultimately possess proper mechanical or chemical stimulation capability [6]. Furthermore, as tendons are regularly subjected to continuous action of tensile loading from muscle contraction, their development and regeneration is closely related to tensile mechanical loading. To tissue engineering a tendon tissue, mechanical stimulation during cell culture has been proved to improve the biological outcomes and mechanical properties of the scaffold/cell construct [7].

Various scaffolds fabricated from different biomaterials have been suggested to resemble the tendon architecture and to achieve the unique biomechanical properties of tendons. The scaffold topography and morphology is crucial for successful regeneration of a tendon. Specifically, fiber-fabricating techniques as well as textile processes have been

employed to engineer and generate fibrous constructs for tendon tissue development [8]. The use of micrometer-scale yarn is one of the methods [9], where textile-based scaffolds could uniquely combine size, shape, load-bearing and strength-retention abilities for tendon repair [10, 11]. However, those textile scaffolds generated from microfiber yarns are different from the inherent nanoscale organization of collagen fibrils in native tendon ECM. This could result in reduced cellular activity and inferior regeneration outcomes [12-14]. Polymeric fibers can be fabricated into different sizes and shapes to meet specific mechanical and biological requirements as an ideal tissue engineering scaffold. Textile techniques like knitting, weaving, braiding etc. can further process the fibers into a more complex 3D structures. Also, the mechanical properties of the scaffolds can be easily modulated through changes in parameters like fiber diameter, angle of braiding, bundle number and morphology of bundles [15]. Although microfibers are good candidate for tendon scaffold/graft development in terms of mechanical stability, their biological activities are not sufficient to achieve effective regeneration. Some of the non-degradable synthetic materials used before for this purpose, e.g. polyethylene terephthalate (PET), polytetrafluoroethylene (PTFE) and polypropylene (PP), were only met with limited success due to this deficiency [16, 17]. From this perspective, designing a fibrous scaffold from biodegradable polymers with relatively small fiber diameter but with high mechanical strength would be preferred, as improved biological activities were reported by using smaller fiber size [18]. Furthermore, electrospun aligned fibers that have the anisotropic structure like collagen fibers in a tendon are more advantageous when used for tendon tissue engineering, due to their ability to effectively propagate mechanobiological cues in an in vivo-like manner [19, 20].

Apart from structural, topographical and mechanical mimicking of a native tendon by a scaffold, the combination of biological components, such as growth factors and cell source, with the developed scaffold should be also considered towards development of a tendon construct [21]. Basic fibroblast growth factor (FGF2), growth and differentiation faction-5, insulin-related growth factor-1, and platelet rich plasma are reported biochemical cues to enhance the ECM production and tensile strength of treated tendons [22]. Considering cell source, tendon-derived cells such as tendon-derived fibroblasts of autologous or allogenic nature will be a suitable choice as a tendon tissue is composed of this cell type. However, properly maintaining tenogenic phenotype in a 3D scaffold during in vitro cell culture still represents a challenging task using this cell source. Other cell sources like bone marrow stem cells and adipose-derived stem cells may be also considered, albeit a suitable niche must be

provided to achieve proper induction into the tenogenic lineage. Considering these facts, a flexible fibrous scaffold, with good mechanical strength, tunable biodegradability and biocompatibility, as well as incorporated with a suitable growth factor, for seeding tendon-derived fibroblasts will be under high demand for the development of a functional tendon tissue.

The present work deals with the combination of all the ideal factors for tendon tissue development, especially the mechanical stability of the scaffold. A slow biodegradable polymer polycaprolactone (PCL) was selected as the base material for the fabrication of sub-micron scale aligned fibers. A commercial suture (Ethicon PDS II 2-0) was chosen as the reinforcing core inside this fibrous layer for its higher mechanical strength. The aligned fiber collected around the suture serve as a sheath to cover the suture in core/sheath structure. The suture-embedded single yarn (SY) could be facilely grafted with heparin for binding FGF2 through bioaffinity interactions. Afterward, three SY were braided to fabricate a multi yarn (MY) scaffold with higher mechanical strength. After comprehensive material characterization, we will carry out in vitro static and dynamic cell culture by seeding rabbit tendon-derived fibroblasts (rTFs) in MY or MY-FGF2 scaffold. A MY-FGF2/rTFs construct after mechanical loading in vitro will be chosen to repair extensor digitorum tendon (EDT) defects in rabbits.

2. EXPERIMENTAL SECTION

2.1 Materials

Polycaprolactone (PCL, molecular weight = 900 kDa), chloroform, methanol, N-hydroxysuccinimide (NHS), heparin sodium salt, Dulbecco's modified Eagle's medium-high glucose (DMEM), (2-(4-amidinophenyl)-6-indolecarbamidine (DAPI) for nuclear staining, phalloidin-tetramethylrhodamine B isothiocyanate (phalloidin-TRITC) for F-actin staining, bisBenzimide H 33258 for DNA quantification were purchased from Sigma-Aldrich. 1-(3-Dimethylaminopropyl)-3-ethylcarbodiimide (EDC) was obtained from Acros. 2-(N-Morpholino)ethanesulfonic acid (MES) and acetonitrile was procured from J.T.Baker. PEG-diamine (molecular weight = 3500) was obtained from Jenkem Technology. HyClone fetal bovine serum (FBS) and Live/Dead viability/cytotoxicity kit for mammalian cells was acquired from Thermo Fisher Scientific. Basic human recombinant fibroblast growth factor (FGF2) was acquired from ProSpec. The Ethicon PDS II (polydioxanone) 2-0 suture was provided by Johnson & Johnson.

2.2 Preparation of scaffolds

2.2.1 Preparation of suture-reinforced single yarn by electrospinning

The spinning solution is 11%(w/v) PCL prepared in chloroform/methanol (7/3 volume ratio). A custom-made electrospinning setup was used for to fabricate suture-embedded PCL fibrous single yarn. Three 10-mL syringes (Terumo) were filled with the PCL solution and placed in a multi syringe infusion pump (KDS 220, KD Scientific). Another 10-mL syringe (Terumo) filled with PCL solution was fitted in a single syringe infusion pump (KDS100, KD Scientific). The syringes in the multi syringe pump were separately connected to three equally placed metallic blunt-edged needles (21 G) in a Teflon disk using silicone tubes, while the syringe in the single syringe pump was directly connected to a metallic needle. Two power supplies for electrospinning were used in the study, with needles from the multi syringe pump connecting to a positive power supply and the needle from the single syringe pump connecting to a negative power supply. Both syringe pumps were kept at ~45° angle towards a metallic plate that is connected to a grounded AC motor. Six metallic rods (15 cm length, 0.8 cm diameter) were equally fixed to the peripheral of the metallic plate at 15° angle for collecting the fibers. A paper cup containing disentwined biodegradable suture (Ethicon PDS II 2-0) was fixed horizontal inside the inner metallic plate of the rotor. A small hole was made at the center of the paper cup and the suture was kept protruded outside the cup, prior to electrospinning. A rotating yarn collector was placed at the other end of the fiber collector to collect a yarn on its rod. The spinning solution was delivered at 4 mL/h flow rate by both syringe pumps at 20 kV, which produced both negatively-changed and positively-changed fibers. The fibers were continuously deposited and twisted in clockwise direction by rotating the metallic plate at 50 rpm to achieve an inter-twisting fibrous environment. The suture protruding from the paper cup was further hooked to a sharp wooden stick and then slowly extended towards the yarn collector. The distance between the metallic fiber collector and all syringe needle tips were at an optimized value of 5 cm for best fiber coverage over the continuously extending suture. The paper cup with the disentwined suture was designed to release the twisting tension generated on the protruding end of the suture to the other end, through free rotation inside the cup. A suture covered with slightly twisted fibers could be pulled towards the rod in a yarn collector rotating at 2.5 rpm for collection of suture-reinforced single yarn (SY) (0.4 mm diameter), using 70-cm long suture in a single run **(Figure 1, Step 1)**.

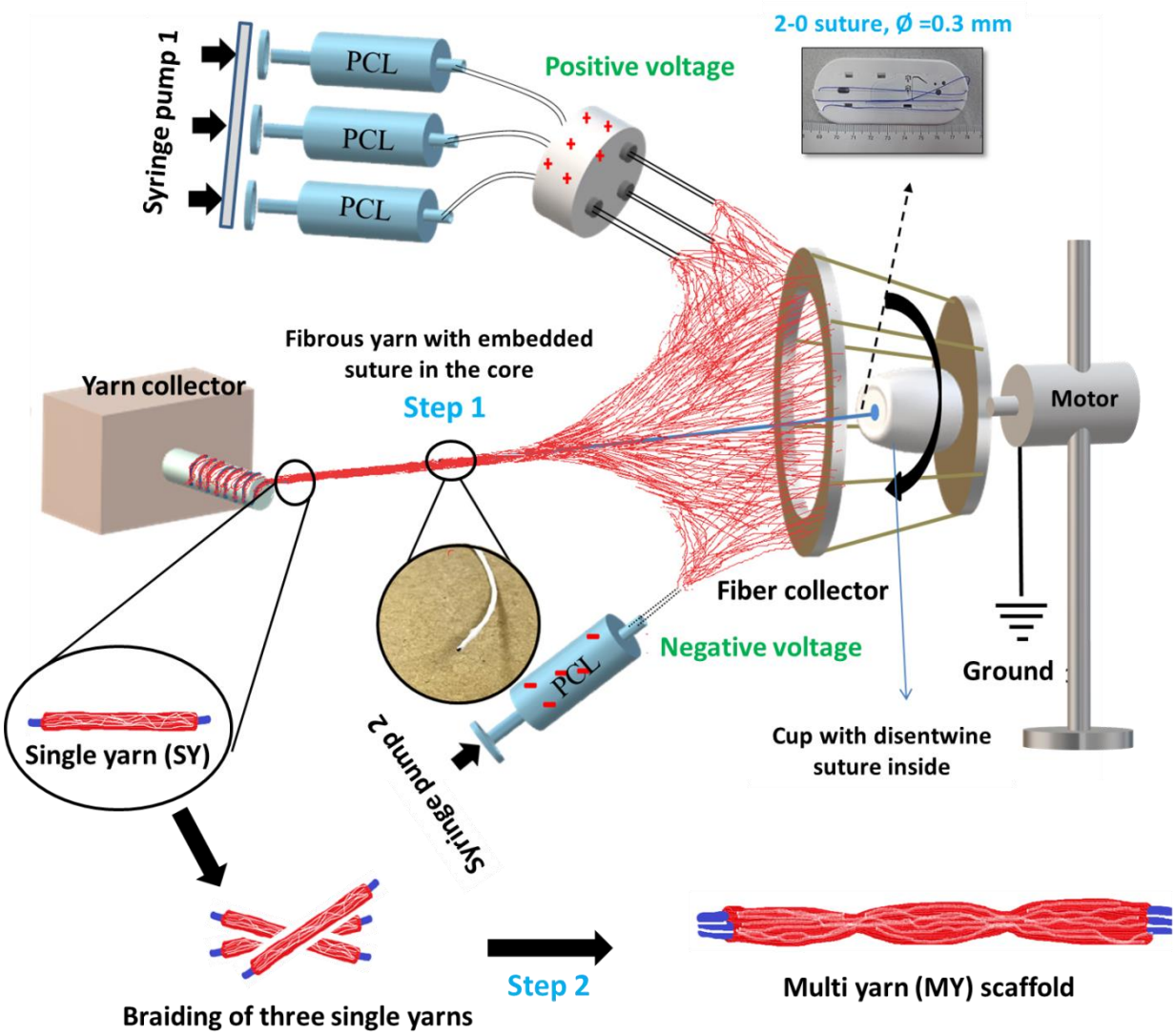

Figure 1. A schematic diagram showing the electrospinning process to obtain suture-reinforced single yarn (SY) covered with aligned PCL fibers, and braiding of three SY to obtain multi yarn (MY) scaffolds.

2.2.2 Braiding of suture-reinforced single yarn (SY) to get multi yarn (MY) scaffold

During this process, three SY were selected in equal length and kept together as a bundle. One end of the bundle was fixed on a clip and further braided to the other end to obtain a braided fibrous multi yarn (MY) scaffold with 0.1-cm knots **(Figure 1, Step 2)**. The MY scaffold was cut into a suitable length and both ends were tied with Nylon 5-0 sutures to prevent un-winding of yarns.

2.2.3. FGF2-conjugated multi yarn (MY-FGF2) scaffold

The MY scaffold was modified in multiple steps for FGF2 conjugation (**Figure S1, Supplementary Materials**). The scaffold was first subject to plasma testament in a DC-pulsed plasma system for surface activation of MY [23]. A customized bipolar electrode

device was used for the surface treatment. MY was cut into 1-cm length prior to the experiment and treated with oxygen plasma generated from a SPIK 1000A oxygen plasma generator at 600 V and 200 mTorr for 120 s to obtain plasma-treated MY (PMY). The PMY was incubated in 0.5 M MES buffer (pH 7) containing 1 mg EDC and 1 mg NHS to activate the carboxyl groups on PMY surface, followed by adding 3 nmol of PEG-diamine. The PEG binding process was carried out for 24 h to obtain MY-NH_2. In order to conjugate heparin, MY-NH_2 was further reacted with 1.2 nmol heparin in EDC/NHS solution prepared in MES buffer for 24 h, similar to PEG-diamine conjugation. The heparin-bound scaffold (MY-H) was washed and placed in an UV box (100 μJ/cm^2) for 4 h on each side for sterilization. The sterilized MY-H was immersed in sterilized FGF-2 solution prepared in phosphate buffered saline (PBS) (2 μg/mL) for 24 h and washed with PBS and water repeatedly to obtain FGF2-conugated MY (MY-FGF2) scaffolds.

2.3 Characterization of scaffolds

2.3.1 Quantification of carboxyl group on PMY

A dried PMY was weighed and immersed in 1 mL of 0.5 mM Toluidine Blue O (TBO) at room temperature for 5 h, followed by washing with 0.01 M NaOH and drying in a vacuum oven at 37 °C to complete dryness. The dried sample was taken out and treated with 2 mL 50%(v/v) glacial acetic acid for complete desorption of TBO. The solution absorbance was measured using an UV/ VIS spectrometer at 633 nm. The concentration of carboxyl groups on the surface of the scaffold was measured from a standard curve of TBO assuming 1:1 binding ratio of carboxyl groups with TBO.

2.3.2 Quantification of amine groups on MY-NH_2

To quantify the amine group on MY-NH_2 surface, 300 μL of 0.25M o-phthaldialdehyde (OPA) was mixed with 4% β-mercaptoethanol prepared in 0.1 M $Na_2B_4O_7$ (pH = 9.5), and made up to 75 mL using distilled water to obtain 1 mM OPA solution. Another solution was prepared by mixing 500 μL of 0.06 M glycine with 500 μl of 0.5% β-mercaptoethanol, and made up to 30 ml using distilled water to reach a final glycine concentration of 1 mM. An OPA standard curve was made from 0.1 mM to 1 mM. A MY-NH_2 (1-cm length) was put inside a glass bottle containing 1 mL of OPA solution. The bottle was shaken for 10 min followed by collecting 50 μL of the supernatant. One mL of 0.1 M $Na_2B_4O_7$ and 100 μL of glycine solution were mixed with the supernatant for 10 min. The solution absorbance was determined with an UV/VIS spectrometer at 340 nm to estimate the

concentration of reacted OPA. The number of -NH_2 group on MY-NH_2 surface was estimated by assuming 1:1 binding ratio between OPA and -NH_2.

2.3.3 Quantification of heparin on MY-H

After reacting heparin with MY-NH_2, the supernatant was collected and analyzed by high performance liquid chromatography (HPLC) for unreacted heparin. A HPLC system was used to determine the absorbance at 210 nm using KH_2PO_4/acetonitrile/methanol = 72/18/10 (v/v) as the mobile phase at a flow rate of 0.5 mL/min. An Eclipse XDB-C18 reverse phase HPLC column (250 mm x 4.6 mm) was used.

2.3.4 Quantification of FGF-2 grafting on MY-FGF2

The quantitative estimation of surface grafted FGF2 on MY-FGF2 was achieved by determining the FGF2 concentration in the washing solution with a commercial human bFGF ELISA kit (RayBiotech ELH-bFGF). To visualize the distribution of surface-grafted FGF2, MY-FGF2 was treated with anti-FGF2-FITC antibody (4 μg/mL) for 1 h and observed under a confocal microscope (Leica TCS SP2), after washing in PBS.

2.3.5 Morphology of scaffold by scanning electron microscopy

The surface morphology of fibrous yarns after each surface attachment/grafting step was observed under a scanning electron microscope (SEM, Hitachi S3000N). The sample was fixed onto a carbon tape pasted on aluminum stub and sputter coated with gold for 60 s at 20 mA. The surface morphology, thickness of fiber deposition and fiber alignment were observed at 15 kV and the respective images were compared with its physical structure.

2.3.6 X-ray spectroscopy (EDS) and X-ray photoelectron spectroscopy (XPS)

The surface elemental composition was analyzed using a scanning electron microscope (SEM, JEOL JSM-7500F) equipped with energy-dispersive X-ray spectroscopy (EDS, Bruker AXS-5030). Surface treated scaffolds were allowed to undergo elemental detection to confirm successful surface modification. The surface chemical composition was also verified through X-ray photoelectron spectroscopy (XPS). A Physical Electronics PHI 1600 ESCA photoelectron spectrometer having a spherical capacitor analyzer and a multi-channel detector was used for the study. The binding energy from 0 to 1300 eV was recorded.

2.3.7 Thermogravimetric analysis

Thermal properties were evaluated by thermogravimetric analysis (TGA) (TGA 2050, TA Instruments). The samples were heated in nitrogen environment at 10 °C/min heating rate from 30 to 700 °C. The TGA thermograms were recorded as weight (%) vs temperature (°C).

The derivative thermogravimetric (DTG) curves are presented as derivative weight (%/°C) vs temperature (°C).

2.3.8 Mechanical properties

The mechanical properties of MY and MY-FGF2 scaffolds were tested through tensile mechanical testing. Both ends of a 1.5-cm long sample were fixed in a metallic grip holder to get a gauge length of 1 cm. A tensile testing machine (Bose ElectroForce BioDynamic) was used to measure the mechanical properties of MY and MY-FGF2 at 0.2%/s strain rate.

2.4 In vitro studies

2.4.1 Isolation of rabbit tendon-derived fibroblasts (rTFs)

The rabbit tendon-derived fibroblasts (rTFs) was isolated from New Zealand white rabbits (8-10 weeks old and 3.0-4.0 kg), as reported earlier with slight modification [24]. All procedures were approved by the Institutional Animal Care and Use Committee of Chang Gung University. Rabbits were sedated using intra-muscular injection of ketamine (10 mg/kg) and xylazine (3 mg/kg). After sacrificing the animals, their flexor tendons were dissected by cutting the tendon tissues 5-mm from the tendon-bone insertion and tendon-muscle junction. The tendon sheath and paratenon were removed and the isolated tendon tissues were weighed and minced into small pieces. Tissue samples were digested in collagenase/dispase solution prepared in PBS at 37 °C for 1 h. The suspension was centrifuged at 1,500 g for 15 min and the pellet was re-suspended in DMEM containing 20% FBS, 1% penicillin-streptomycin and 3.7 g/L sodium bicarbonate. The suspension was transferred to T75 flasks and incubated in a CO_2 incubator at 37 °C for two weeks for migration of rTFs to the culture plate surface. The rTFs was detached through 0.05% trypsin/EDTA treatment and sub-cultured in T-75 flasks with medium change every three days.

2.4.2 Static culture of rTFs in MY and MY-FGF2

The MY or MY-FGF2 with 1-cm length were sterilized by UV light or 4 h at 100 $\mu J/cm^2$ on each side and pre-wetted with cell culture medium prior to cell seeding. A 10-µL cell suspension containing 1×10^5 rTFs was seeded to each scaffold. After 4 h of cell seeding, 2 mL DMEM was added to immerse the sample and cell culture was carried out in a CO_2 incubator at 37 °C with medium change every three days.

2.4.3 Morphology, viability and cytoskeletal arrangement of rTFs on MY and MY-FGF2

After culture for different times, a cell-seeded scaffold was fixed in 2.5% glutaraldehyde for 30 min and followed by PBS washing. A gradient alcohol washing was given to remove water content from the sample, which is further vacuum dried. The morphology of adhered cells was examined through SEM (Hitachi S-3000N). The viability of rTFs in the scaffold was determined through Live/Dead assays [25]. At each time point, the samples were stained with calcein AM/ethidium homodimer in a Live/Dead viability/cytotoxicity kit. All samples were washed with PBS after staining and observed under a confocal laser scanning microscope (Zeiss LSM 510 Meta) at excitation/emission wavelength of 494 nm/517 nm for live cells, and excitation/emission wavelength of 528 nm/617 nm for dead cells. To observe cytoskeletal arrangement, the samples were fixed with glutaraldehyde, followed by permeabilization in 0.1% Triton X-100 for 10 min at room temperature. Thereafter, they were stained with red fluorescence-producing phalloidin-TRITC (1 µg/mL) for 30 min, and blue fluorescence-producing DAPI (1 µg/mL) for 10 min. The orientation of actin microfilaments in adhered rTFs was visualized through a confocal laser scanning microscope (Zeiss LSM 510 Meta) at excitation/emission wavelength of 540 nm/545 nm for phalloidin-TRITC and excitation/emission wavelength of 358 nm/461 nm for DAPI.

2.4.4 Cell proliferation

The cell seeded scaffold was removed from the culture plate and washed three times with PBS at pre-determined time points. The samples were then immersed in 1 mL digestion buffer (55 mM sodium citrate, 150 mM sodium chloride, 5 mM cysteine, 5 mM EDTA and 0.2 mg/ml papain) by shaking at 60 °C for 24 h. The solution was centrifuged at 20 °C for 5 min, and 10 µL of supernatant was mixed with 200 µL of 10 mg/ml bisBenzimide H 33258 solution. The fluorescence intensity was measured using an ELISA reader (Synergy HT, BioTek) [26].

2.4.5 Gene expression

The gene expression of type I collagen (COL I), type III collagen (COL III), tenacin C, biglycan and fibronectin were examined using standard protocols for RNA isolation and cDNA synthesis.[27] The quantitative real-time polymerase chain reaction (qRT-PCR) was performed using a SYBR® Green RT-PCR kit (SYBR Green I supermix) with a MiniOption detection system (Bio-Rad CFD-3120). The glyceraldehyde 3-phosphate dehydrogenase (GAPDH) was used as a housekeeping gene for internal control. The gene expression analysis was carried out using the $2^{-\Delta\Delta Ct}$ relative quantification method and reported as relative

expression by normalizing the relative mRNA content for each gene with its respective value on day 0. The primers used for the study are listed in **Table S1** (**Supplementary Materials**).

2.4.6 Immunofluorescence staining

For immunofluorescence (IF) staining of COL I and tenascin C, the samples were rinsed with PBS and fixed with 4% paraformaldehyde in PBS for 30 min, followed by washing with PBS/0.1% Tween 20 (PBST) for 3 times (15 min each). The sample was treated with 1 mL of HyBlock 1-min Blocking Buffer and washed by PBST. The COL I (1:2000 in PBST, mouse monoclonal anti-COL I, Abcam, USA) and tenacin C primary antibodeis (1:1000 in PBST, mouse monoclonal anti-tenacin-C, Abcam, USA) were separately reacted with each sample for 24 h at 37 °C. The sample was further washed with PBST and incubated with goat anti-mouse IgG-FITC secondary antibody (1:200) (Jacksons Laboratories) for 2 h. The incubation was terminated by PBST washing and further stained with DAPI (1 μg/mL) for 15 min for nuclear stain. The samples were exxamined under a Leica TCS SP2 laser scanning microscope (Wetzlar, Germany) and imaged using excitation/emission wavelength of 490/519 nm for FITC and 358/461 nm for DAPI, respectively. A semi-quantitative analysis of COL I and tenacin C was performed through the area percentage of the green fluorescence signal corresponding to COL I or tenacin C in each image using the PAX-it!^{TM} image analysis software,.

2.4.7 In vitro dynamic cell culture

For dynamic cell culture, the MY-FGF2 scaffold was selected and followed the same sterilization and cell seeding procedures as described before for static cell culture. A 1.5-cm length MY-FGF2 scaffold was fixed horizontally from both ends to clamps provided in a bioreactor (BioDynamic 5100 single specimen mechanical stimulation bioreactor, TA Instruments), leaving 1-cm length for seeding 1×10^5 rTFs [28]. After 4 h, the bioreactor was filled with 175 mL of cell culture medium for cyclic tensile loading of the MY-FGF2/rTFs construct in a CO_2 incubator at 37 °C and 5% CO_2. The construct was mechanically stimulated 3 h per day at 0.5 Hz frequency, and with 0, 3 or 5% strain. After dynamic culture for 7 days, the sample was removed from the bioreactor and subject to analysis following the same experimental methods and analytical procedures as described above for static culture.

2.5 In vivo studies

The regeneration efficiency of the mechanical stimulated MY-FGF2/rTFs construct was tested in extensor digitorum tendon (EDT) defect model in rabbits as per the animal

ethics protocols approved by the Institutional Animal Care and Use Committee of Chang Gung University. For rabbit implantation studies, eight 6-8 month old New Zealand white rabbits were selected and divided into two groups, viz., cellular and acellular groups. A 1.5-cm MY-FGF2 scaffold was dynamically cultured with 1×10^5 rTFs at 5% strain for 7 days as in dynamic cell culture and used as the cellular group. A 1.5 cm MY-FGF2 scaffold treated in the same way in the bioreactor was used as the acellular group. The rabbits were anesthetized by intramuscularly injecting 1:1 combination of Zoletil 50 and Rompun. Continued inhalation of isoflurane was used to maintain the rabbit under anesthetic condition throughout the experiment. The rabbit's legs were shaved, the muscles were opened and the EDT was exposed. The tendon defect was created by removing 1-cm length ETD from both legs of the animal. A cellular sample was implanted to the animal's left leg while an acellular sample was implanted to its right leg, by suturing both ends of the scaffold separately to the proximal and distal ends of the native tendon. The surgical sites were closed with nylon sutures and cefozolin sodium was applied to the animal as a prophylactic antibiotic. The wound was dressed with biomycin ointment to prevent infection. All animals were euthanized 6-week post-implantation and the implant site was exposed using a scalpel. The sample was retrieved by cutting at both ends of the native tendon and soaked in 10% formaldehyde for histological analysis and in PBS for biomechanical tests. For histological analysis, paraffin-embedded samples were sectioned for hematoxylin and eosin (H&E) staining, Masson's trichrome staining, and immunohistochemical (IHC) staining of COL I, Col III and tenascin C. For biomechanical tests, samples from acellular and cellular groups as well as native rabbit ETD were subject to tensile mechanical testing (Bose ElectroForce BioDynamic) at 0.2%/s strain rate.

2.6 Statistical analysis

The data are presented as mean ± standard deviation. The one-way analysis of variance (ANOVA) with the least significant difference (LSD) test was used for statistical analysis. A p value less than 0.05 is considered statistically significant.

3. RESULTS AND DISCUSSION

3.1 Fabrication and characterization of scaffolds

The suture-reinforced single yarn (SY) was prepared as shown in **Figure 1**. The whole set up has been optimized to uniformly and fully cover a 2-0 commercial suture with aligned

PCL fibers as a sheath. Using three needles connected to a positive power supply for electrospinning, continuously deposition of PCL fibers on the surface of an extending suture in possible. For continuous fiber collection, another needle connected to a negative power supply was placed vertically from other needles, for collecting electrospun PCL fibers with from electrostatic force generated from opposite surface charge. The combined use of both positive and negative power sources hence can drive most of the fiber stream to the center of the collection drum. The twisting of collected fibers on top of the extending suture can enable efficient wrapping to entrap the suture within a single yarn. High-strength surgical sutures with 300-μm diameter were selected here for the reinforcement of tendon scaffolds. Though the suture inside the paper cup was revolving during drum rotation, the disentwined nature of the suture resulted in free rotation of the suture terminal inside the cup, releasing the strain experienced during electrospinning. The length provided by a single surgical suture was 70 cm, and its disentwined nature could be properly maintained throughout the process without strain development for getting a single yarn (SY). The SY could be facilely collected with a rotating rod fitted in a yarn collector. The rotation speed of the collection drum, flow rate of the solution, and voltage for electrospinning has been optimized beforehand to obtain uniform fiber deposition. Compared to non-woven and aligned fibrous structure fabrication, some reports are available on yarn fabrication through electrospinning, whereas a dynamic liquid support system was reported for continuous electrospun yarn fabrication [29]. A more similar method of yarn fabrication was later reported as direct electrospinning [30]. However, combination of a biodegradable suture and fibrous structure is developed here for the first time to achieve higher mechanical stability, which is much relevant for tendon scaffold fabrication.

The morphology of SY and braided MY scaffold examined under SEM reveals uniform fiber deposition on suture surface (**Figure 2A and B).** A suture-embedded SY could be prepared with 0.5 mm diameter, while braiding of three SY produces a bundled MY scaffold of 1.25 mm diameter. The fibrous layer on the surface of SY and MY shown from the SEM images reveals somewhat aligned fiber morphology by collecting with a rotating fiber collector (**Figure 2C and D**).

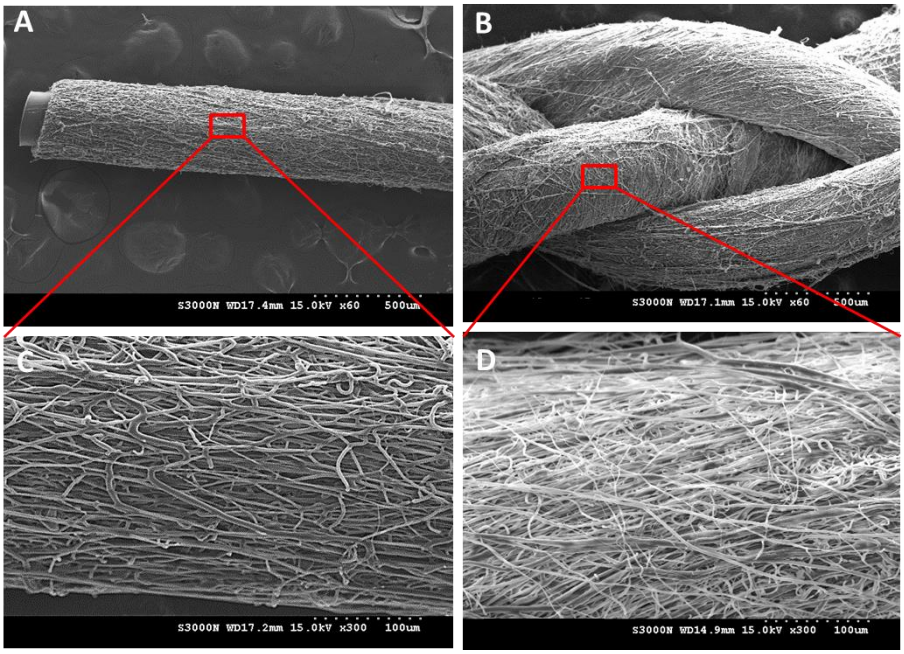

Figure 2. The scanning electron microscopy images of suture-reinforced single yarn (SY) covered with PCL fibers (A and C), and multi yarn (MY) scaffolds from braiding of three SY (B and D).

As plasma treatment was used to generate carboxyl groups on MY surface to facilitate grafting of PEG-diamine, the optimum treatment duration to achieve maximum surface-grafted carboxyl groups must be studied. For this purpose, plasma treatment was carried out for different periods and the amount of carboxyl groups on the surface of PMY was measured using the TBO assay method **(Figure S2, Supplementary Materials)**. The untreated sample showed background carboxyl groups at 0.12 ± 0.01 nmole/mg. The 60-s and 90-s plasma-treated samples displayed 0.51 ± 0.01 nmole/mg and 0.52 ± 0.03 nmole/mg contents, with no significant difference. When treated for 120 s, the content increased to 0.61 ± 0.01 nmole/mg and the value is significantly higher than those at 60 and 90 s. However, further increase of treatment time to 180 s resulted in similar –COOH concentration with that observed for 120 s. Taken together, we chose 120 s as the optimum plasma treatment time to prepare PMY.

When PEG-diamine reacted with PMY in the presence of EDC/NHS, the carboxyl groups on PMY surface was activated, which can form amide bonds with the primary amine groups in PEG-diamine to yield MY-NH_2. To conjugate just one amine group in PEG-diamine to PMY while leaving the other amine group available for further reaction, we used a PEG-diamine concentration providing a 5 to 1 ratio of –NH_2 to –COOH during the reaction. This process produced MY-NH_2 with 0.461± 0.018 (nmole/mg) free amine groups from the OPA assay. During the next heparin conjugation step, the EDC/NHS caused the activation of

carboxyl groups in heparin and formed amide bonds with free amine groups in MY-NH_2. The dose of heparin used (~1.2 nmole) was controlled at 2.5 times that of free amine groups in MY-NH_2 to obtain heparin-conjugated MY (MY-H). The heparin concentration on MY-H surface was 0.585 ± 0.025 (nmole/mg) from unreacted heparin in the supernatant after reaction. The scaffold surface during the surface modification steps are characterized by SEM and included in **Figure S3 (Supplementary Materials)** for PMY, MY-NH_2 and MY-H. The surface morphology of the yarns is found to be un-altered irrespective of successive surface modification. The fiber topography was maintained and thus the yarn bundles maintained its physical stability. It is also important to note that the inter- and intra-yarns spaces are highly visible and thus it would be of great potential in terms of tissue engineering aspects.

The EDS spectrum and the elemental composition of MY, PMY, MY-NH_2 and MY-H is shown in **Figure S4 (Supplementary Materials)**. Only C and O elements were detected on MY surface as expected. After plasma treatment, the atomic percentage of O increased from 11.97% (MY) to 13.28% (PMY). It is inferred that oxygen plasma modification will increase the carboxyl groups on the surface of the fibrous yarn scaffold, leading to increased oxygen content. The successful introduction of amine groups was confirmed from the presence of abundant nitrogen elements in the EDS spectrum of MY-NH_2 with 15.48% atomic percentage. Finally, it could be clearly observed that after heparin conjugation, sulfur and sodium start to show in the EDS spectrum of MY-H, with 0.11% and 0.04% atomic percentages, respectively. Since heparin is a highly sulfated glycosaminoglycan and heparin sodium salt was used here, we confirm successful surface conjugation of heparin to the scaffold, which could be used for FGF2 binding.

X-ray photoelectron spectroscopy (XPS) is the energy analysis of surface generated photoelectrons by x-ray irradiation. This photoelectron spectrum displays the characteristic peaks for all elements except H and He, which can be used to identify the surface elements qualitatively and quantitatively. Even minor shifts in peak positions implies the chemical binding state of elements on the surface and thus the technique was used to examine the chemical composition of the elements on the surface of the scaffolds. **Figure 3A** is the ESCA analysis of MY, PMY, MY-NH_2 and MY-H, where C (286 eV) and O (534 eV) are the common elements observed in all samples. Nitrogen in MY-H exhibited a peak at 401 eV with an additional peak at 495 eV. It can be seen that the signal intensity of oxygen in PSY is higher than that in MY after oxygen plasma treatment. The atomic percentage data justifies the phenomenon where carbon percentage in PSY reduces to 73.44% from 83.53% in MY,

while oxygen content increases to 26.56% in PMY from 16.47% in MY. It is speculated that oxygen plasma modification increased the content of carboxyl groups on the surface of PMY and lead to an increase in oxygen content percentage. When PMY was further surface modified with amines, the nitrogen binding peak appeared on MY-NH_2 surface with a nitrogen atomic percentage of 1.77%, which does not appear in PMY. This infers to the successful amine binding in MY-NH_2. After heparin modification on MY-NH_2, the resultant MY-H sample displayed both the peaks of sulfur and sodium, evident from the atomic percentage values of 1.39% for Na and 1.05% for S. The nitrogen atomic percentage in MY-H is 1.27% and lower than that of MY-NH_2, due to the surface coverage of heparin over PEG-diamine, as has been reported previously [31].

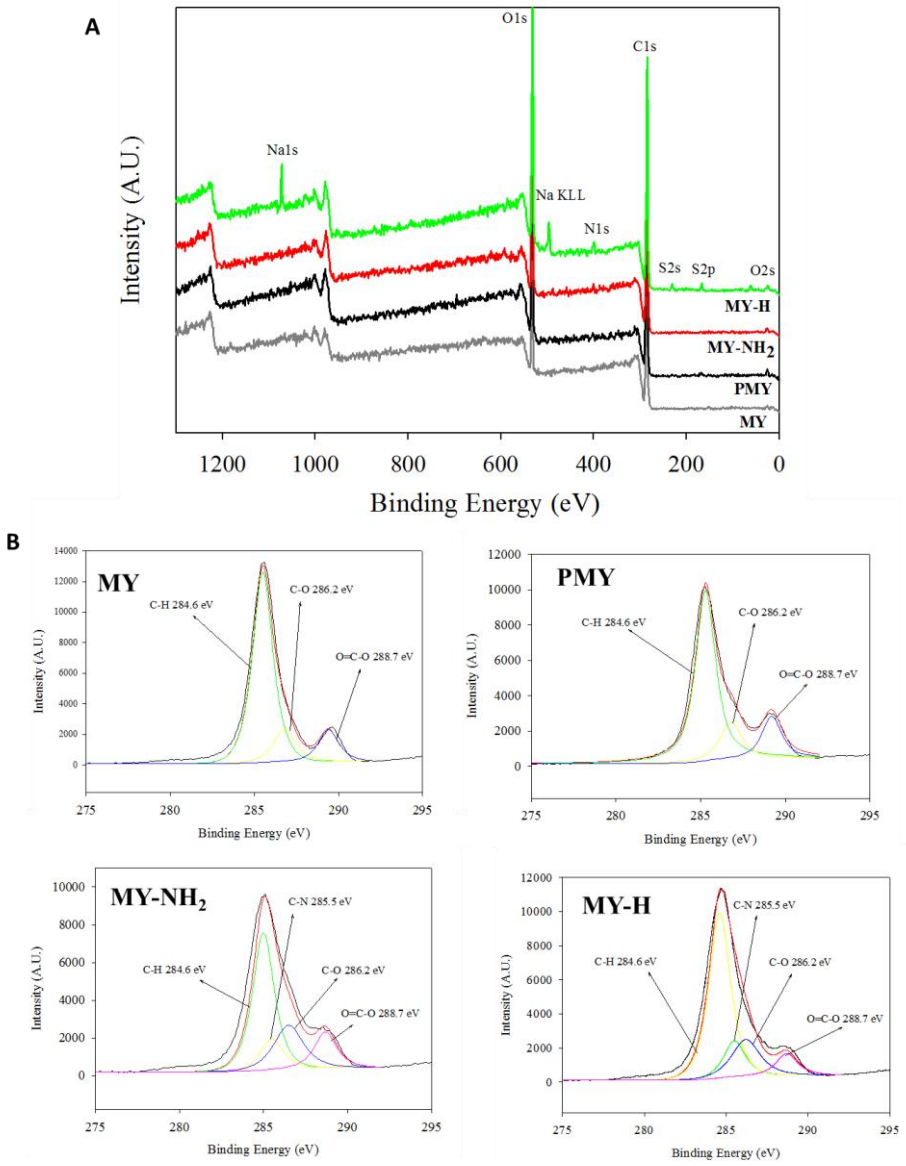

Figure 3. The XPS survey scan spectra (A), and the XPS C1s spectra (B) of MY, PMY, MY-NH_2 and MY-H.

The fractions of various carbon functional groups were further calculated from high-resolution XPS C1s spectra (**Figure 3B**), and the corresponding values are reported in **Table 1**. The four peaks at 284.6, 286.2, 288.7 and 285.5 eV correspond to the C–H, C–O, and O=C–O and NH-C=O bonds in the PCL chain [32]. It is observed that the C-H content in MY decreased after oxygen plasma treatment with concomitant increase of C–O and O–C=O contents in PMY **(Table 1)**. From the respective C1s spectra of MY-NH_2, the formation of amide bonds resulted in the decrease of O–C=O content from 16.47% in PMY to 13.92% in MY-NH_2 (**Table 1**). A NH–C=O peak appears in MY-NH_2 at 11.97%, confirming amide bond formation during introduction of –NH_2 groups using PEG-diamine. After heparin conjugation, the O–C=O content further reduced to 7.79% and the NH–C=O content increased to 13.24% in MY-H, confirming amide bond formation between heparin and amines groups in MY-NH_2. Taken together, the surface chemistry during the successive modification steps of MY to MY-H could be confirmed.

Table 1. Fraction of carbon functional groups from high resolution C1s XPS peaks.

Sample	C–H ~284.6 eV (%)	C–O ~286.2 eV (%)	O–C=O ~288.7 eV (%)	NH–C=O ~285.5 eV (%)
MY	74.29	13.56	12.15	0.00
PMY	67.20	16.32	16.47	0.00
MY-NH_2	52.16	21.95	13.92	11.97
MY-H	61.41	17.55	7.79	13.24

Thermogravimetric analysis (TGA) is used to understand the effect of temperature, rate of decomposition and thermal stability of different polymeric materials when heated. It was used to analyze the thermal properties of MY and MY-H, from which components in the yarn bundles, i.e. sutures, PCL and heparin, could be confirmed. From TGA (**Figure S5A, Supplementary Materials)** and derivative thermogravimetric (DTG) curves **(Figure S5B, Supplementary Materials)**, suture and PCL showed similar single stage decomposition pattern with onset thermal decomposition temperatures of 295 °C and 401 °C, respectively. Quantitative decomposition was found for suture and PCL at 500 °C, due to their synthetic polymer nature. The onset decomposition of MY was slightly higher than suture but significantly lower than PCL, confirming the combined effect from both suture and PCL. The steep decomposition of MY follows the same trend as suture until loosing 80% weight, followed by a second-stage milder weight loss till 404 °C and finally attained 100% decomposition. The two-stage thermal decomposition pattern shown by MY leads to two

decomposition peak temperatures that could be assigned to suture and PCL, as observed from the DTG curve. Being a mixture of sulfated polymers of carbohydrates sugar molecule, heparin doesn't follow the decomposition characteristics of other synthetic polymers (suture and PCL) in MY-H, and hence there was no sharp onset of decomposition. Heparin disintegrated in a straight temperature proportion and retained 32% residual weight even after 700°C. Interestingly, MY-H showed mix properties of PCL, suture and heparin in its decomposition pattern. The onset decomposition was identical to MY till 315 °C, followed by a minor second-stage decomposition with a doublet peak temperature at 324 °C. Even after 700 °C, 7% residual weight of MY-H remains, which is not found for suture, PCL and MY. Based on the results, it is inferred that heparin has been successfully grafted to the surface of MY-H scaffold.

Successful binding FGF2 to MY-H was confirmed from confocal microscopy observation. The control sample MY-H did not show any fluorescence signal due to the absence of FGF2 while MY-FGF2 displays sporadic green fluorescence signals from binding of FITC-labelled anti-FGF2 antibody to FGF2 on MY-FGF2 surface (**Figure S6A, Supplementary Materials)**. The distribution of FGF2 within a MY-FGF2 scaffold is also evident by the comparing the SEM and confocal microcopy images (**Figure S6B, Supplementary Materials)**. From ELISA quantification of unbound FGF2 after reacting one MY-H scaffold with 2 μg FGF-2, the amount of FGF2 bound to MY-H was almost quantitative at 1.98 ± 0.01 μg per MY-FGF2 scaffold. Undoubtedly, the high binding efficiency is due to the strong bioaffinity between heparin and FGF-2, where a dissociation constant as low as 109 nM was reported [33]. Apart from protein binding, heparin can also protect FGF-2 from proteolysis from in vitro and in vivo studies [34]. Furthermore, heparin also modulates the mitogenic activity of FGF2 by inducing the dimerization of the FGF-R2 receptor [35]. Therefore, a 3D scaffold containing immobilized heparin could be employed for the long-term anchoring of bioactive FGF2 to mediate cellular response of rTFs for tendon tissue engineering.

As mechanical property is an important consideration of a tendon tissue engineering scaffold, we used tensile mechanical testing to characterize MY and MY-FGF2 to elucidate the effects of successive modification steps on their mechanical properties. The force-displacement curves were used to calculate the stiffness, toughness, ultimate force and ultimate displacement of MY and MY-FGF2 (**Figure S7, Supplementary Materials)**. No significance changes of mechanical properties was found between them, implies surface

plasma modification, chemical grafting of PEG-diamine and heparin, and physical binding of FGF2 did not affect the mechanical stability of the suture-embedded scaffolds. The ultimate displacement of ~1.7 mm occurred at the ultimate force in both MY and MY-FGF2 is considered to be more suitable for resisting high tensile forces with limited elongation, as reported for tendon mechanics [36]. The maximum strain calculated form the ultimate displacement is 17%, which has been set as the strain limit during cyclic mechanical loading of MY-FGF2 during dynamic cell culture.

3.2 In vitro studies: static culture

Using scanning electron microscope (SEM) to observe rTFs grown in MY and MY-FGF2, **Figure 4A** reveals the cell morphology on day 0, 7, 14 and 21. Both scaffolds exhibit similar cell adhesion pattern without significant differences. The cell density on day 0 and 7 were moderate in both scaffolds, but showed an interpenetrated cellular growth network on day 14 and 21, where cells in MY-FGF2 appears to be more spreading. Cells in MY-FGF2 at day 21 also displayed complete surface coverage compared to MY at the same time point. The cells also show oriented growth pattern in the direction of fibers. The viability of rTFs in both scaffolds were analyzed through the Live/Dead staining at different time points, with the green fluorescence representing live cells and the red fluorescence referring to possible dead cells (**Figure 4B**). Interestingly, both samples exhibited green fluorescence at all time points irrespective of scaffolds. Relatively negligible amount of red stains appeared in the merged images, underlining the biocompatibility of both scaffolds. As observed from SEM images, the density of live cells was moderate on day 0 and 7. The cells appeared as intermittent green spots on day 0 and turned out to be a well-oriented cell layer at later stages of cell growth. The cell layering was more thick and defined for MY-FGF2 in comparison with MY, possibly due to presence of FGF2. In order to validate the advantageous MY-FGF2 towards substrate-specific cell growth, DAPI/phalloidin staining as used to observe cytoskeleton by labelling F-actin in red with phalloidin-TRITC and cell nuclei in blue with DAPI (**Figure 4C).** Consistent with previous SEM observations, time-dependent increase of cellular density is evident and reaching the maximum at day 21, but more cells was found in MY-FGF2. The actin filaments are found oriented along the fiber long-axis in the scaffolds, which may help the rTFs-seeded scaffold to enhance its tensile properties. The DAPI-stained nuclei of MY-FGF2 also charted an axial pattern of adhesion, confirming the successful growth and proliferation of rTFs towards tendon regeneration.

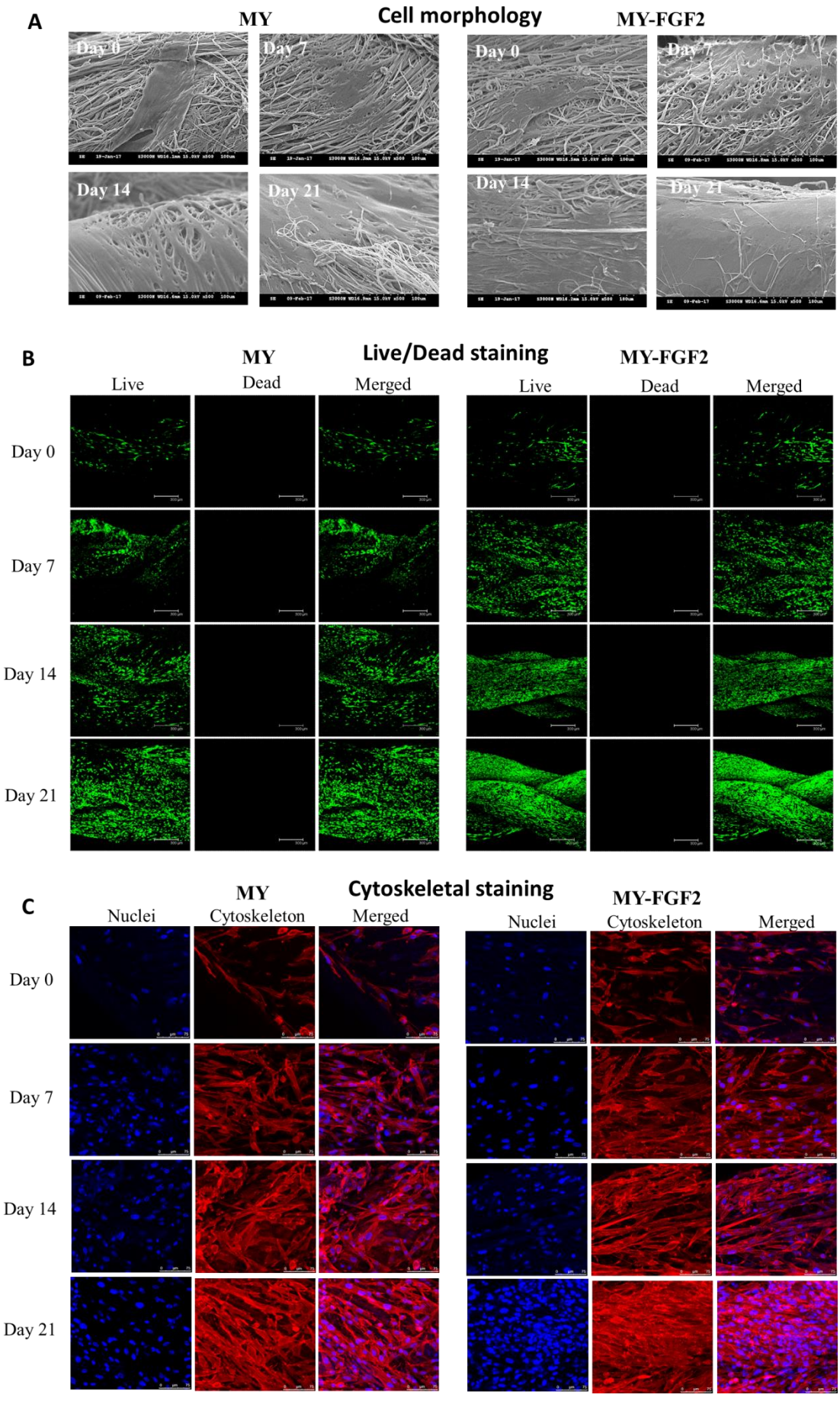
A
MY
Cell morphology
MY-FGF2
Day 0
Day 7
Day 14
Day 21
Day 0
Day 7
Day 14
Day 21
B
MY
Live/Dead staining
MY-FGF2
Live
Dead
Merged
Live
Dead
Merged
Day 0
Day 7
Day 14
Day 21
C
MY
Cytoskeletal staining
MY-FGF2
Nuclei
Cytoskeleton
Merged
Nuclei
Cytoskeleton
Merged
Day 0
Day 7
Day 14
Day 21

601

Figure 4. The microscopy characterization of the rTFs after cultured in MY and MY-FGF2 for 0, 7, 14 and 21 days through scanning electron microscopy (A, bar = 100 μm), and confocal microscopy after Live/Dead (B, bar = 300 μm) and cytoskeletal (C, bar = 75 μm) staining.

The proliferation of rTFs in MY and MY-FGF2 were assessed quantitatively and represented as DNA contents on day 0, 7, 14 and 21in **Figure 5A**. Supporting previous microscopy observation shown in **Figure 4A**, the MY-FGF2 dominated the rate of cell proliferation over MY. For both scaffolds, the cell number increased rapidly with time. There is no significant difference in cell number on day 0, indicating similar cell attachment rate. Nonetheless, there is significant difference in DNA contents on day 7, 14, and 21. This underlines that FGF2 in MY-FGF2 may accelerate cell proliferation, as this growth factor is a well-recognized cell signaling molecule for neo-tendon tissue development during tendon healing [37]. This is also supported from the finding that FGF2 can promote cell mitosis and proliferation [38]. Considering the uniform distribution of FGF2 in MY-FGF2 as revealed in **Figure S6**, the DNA quantification results are affirmative of the bioactivity of FGF2 could be preserved by immobilization to MY-FGF2 scaffold though anchoring to heparin by bioaffiinity binding. It should be noted that the cellular response elicited by FGF2 is irrespective to its free or immobilized form. The release of FGF2 from MY-FGF2 has been followed for 21 days in PBS during this study. However, no FGF2 could be detected in the release medium by ELISA due to the strong binding between FGF2 and heparin.

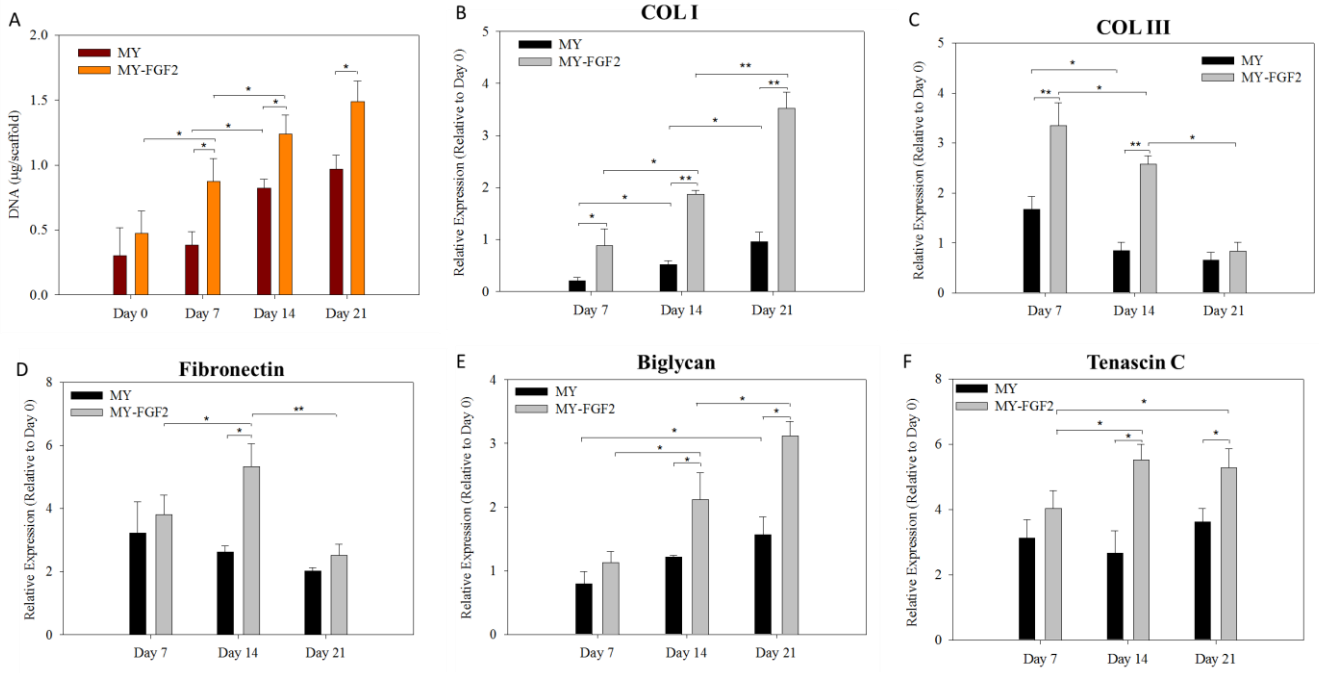

Figure 5. (A) The proliferation for rTFs in MY and MY-FGF2 by measuring the DNA contents per scaffold. (B-F) The gene expression analyses of type I collagen (COL I), tenascin C (C), type III collagen (COL III), biglycan (E), and fibronectin (F) by qRT-PCR.

A critical evidence of rTFs differentiation in presence of FGF-2 is the identification of relevant tenogenic marker genes during in vitro cell culture. During differentiation, rTFs will undergo different transition stages with regulated expression of various marker genes. The relative gene expression of COL I, COL III, fibronectin, biglycan and tenascin C were determining using GAPDH as a housekeeping gene, and normalized with its respective value on day 0 **(Figure 5B-F)**. COL I is the major protein in the ECM tendon tissue, where fibrillar arrangement of triple-helical COL I molecules successively organized into tensile-resistant fibrils, fibers and fiber bundles, and provide major resistance to mechanical forces. It is deemed a late-stage gene marker for tendon repair with increased secretion throughout the whole tendon repair [39]. During 21-day culture period in MY, rTFs show increased gene expression of COL I with time. However, the relative value never exceed one by reaching its initial value on day 0, indicating rTFs could partially recover their lost phenotype when cultured in MY, possible originating from the biophysical cues provided by aligned fibers in the scaffold without FGF2 [40]. Although the COL I gene expression in MY-FGF2 shows similar time-dependent increase as MY, significantly enhancement of mRNA levels over those in MY was found at all time points, suggesting that FGF2 on fiber surface can elicit biochemical cues to affect rTFs. This is consistent with the report that FGF2 can act on the cell surface receptor by phosphorylated it for activating several downstream intracellular secondary messenger molecules, and result in upregulated expression of this tenogenic marker [41].

The COL III is the second most abundant type of collagens in tendon ECM, and found in the endotenon and epitenon regions of normal tendons. When the tendon remodels and develops during healing, COL III will be gradually replaced by aligned and long COL I fibrils. It is an early-stage gene marker during tendon healing [42]. A different gene expression pattern was thus observed for COL III from COL I, with decreased gene expression level with time. Both MY and MY-FGF2 showed early expression of COL III on day 7 with relative gene expression level above 1, endorsing aligned fibrous structural arrangement in the scaffold contribute to expression of this early marker. On day 7 and 14, MY-FGF2 shows a significantly higher level of COL III expression compared to MY, which was not found on day 21. Since COL III is produced during the collagen maturation process, MY-FGF2 may be

suggested to provide a higher collagen maturation rate, which is beneficial for tendon reconstruction. This is supported from insignificant COL III gene expression level difference between both scaffolds on day 21 when approaching tendon maturation.

Like COL III, fibronectin is also an early-stage tendon marker gene with maximal synthesis during cell proliferation, and declined synthesis during cell maturation by affecting early cell attachment and survival [43]. It is a well-known marker for active connective tissue repair and the down-regulation of fibronectin gene expression on day 21 is consistent with its known gene expression pattern where fibronectin synthesis is less as rTFs matured and accumulated collagens [44]. Therefore, significant differences was only observed for this gene on day 14 between MY and MY-FGF2. The MY does not show significant change of fibronectin gene expression level with time. In contrast, the MY-FGF2 shows significant increase of mRNA level early from day 7 to day 14, followed by drastic down-regulation of fibronectin gene expression, indicating FGF2 can promote tendon maturation.

The biglycan is considered as a late maker gene by regulating the action of many growth factors throughout tendon healing, which also regulate the arrangement and diameter of collagen fibrils in the ECM of healed tendon tissues [45]. The gene expression level of biglycan increase slowly with time for MY with significance found only between day 7 and day 21. Nonetheless, MY-FGF2 provides pronounced upregulated biglycan gene expression throughout the culture period and significantly higher expression level was found for MY-FGF2 over MY on day 14 and 21. This again highlights the benefit using the FGF2-loaded MY-FGF2 for rTFs culture in neo-tendon tissue development in vitro. The tenascin C is a unique protein in tendon tissue, which promotes regeneration and restoration of tendons. Hence, gene expression of this protein should be upregulated throughout the growth and maturation phase of tendon tissue. The MY shows increased gene expression of tenascin C from day 14 to day 21. In contrast, continuous gene expression increase for MY-FGF2 is evident with much higher level of mRNA increase from day 7 to day 21. The MY-FGF2 scaffold also significantly upregulated tenascin C gene expression on day 14 and 21 compared with MY. Overall, FGF2-mediated gene expression pattern change could be clearly demonstrated when rTFs were cultured in MY-FGF2, with upregulated expression of all tenogenic marker genes. This implicates the preference use of MY-FGF2 for culture of rTFs in vitro, to provide better maintenance of the tenogenic phenotype.

To complement the gene expression levels determined by qRT-PCR, the synthesis of tendon marker proteins COL I and tenascin C were studied from immunofluorescence (IF)

staining (**Figure 6**). From confocal microscopy observation, the green fluorescence signal is assigned to protein molecules after binding with the FITC-labelled antibody while blue spots are the cell nuclei. The presence of COL I and tenascin C in MY and MY-FGF2 were minimal on day 0, while a moderate staining intensity was observed for both scaffolds on day 7, irrespective of protein types. The proteins start showing increased deposition in the scaffold after day 14, and reaching a much higher protein density on day 21 for both samples. Interestingly, the secreted protein shows orientation possibly following the direction of aligned fibers on day 7 and 14, which has been also found for cytoskeleton expression in **Figure 4C**. The aligned pattern was not noticeable on day 0 due to minimum protein deposition, while on day 21 it may be too thick for clear visualization. Overall, the IF-staining images supports a higher rate of COL I and tenascin C synthesis by rTFs in MY-FGF2. A semi-quantitative evaluation of COL I and tenascin C synthesis was performed by using an image analysis software [46]. The quantified COL I area percentage in IF images at day 0 was 6.9% and 11.0% for MY and MY-FGF2, respectively. An increase in protein deposition rate was observed at later stages, with concomitant increase of stained area percentage to 26.5% (day 7), 38.8% (day 14) and 67.7% (day 21) for MY, and 40.3% (day 7), 66.4% (day 14) and 91.1% (day 21) for MY-FGF2. In a same way, the fluorescence stained areas of tenascin C on day 0, 7, 14 and 21 are 9.0%, 29.6%, 43.7% and 66.7%, respectively, for MY. The values are 14.7%, 43.2%, 60.3% and 94.0% for MY-FGF2. In both cases, MY-FGF2 had higher protein deposition rate compared to MY at each time point. It is also noticeable that the difference in protein deposition rate between MY and MY-FGF2 increases with time. Considering COL I, the difference in protein quantification between MY-FGF2 and MY on day 0 is 4.1%, while it is 23.4% on day 21. Similarly for tenascin C, it is 5.7% and 27.3% on day 0 and 21. Taken together, all these observations confirm the positive effect of MY-FGF2 on cell proliferation, collagen fibril formation and ECM development for tendon regeneration.

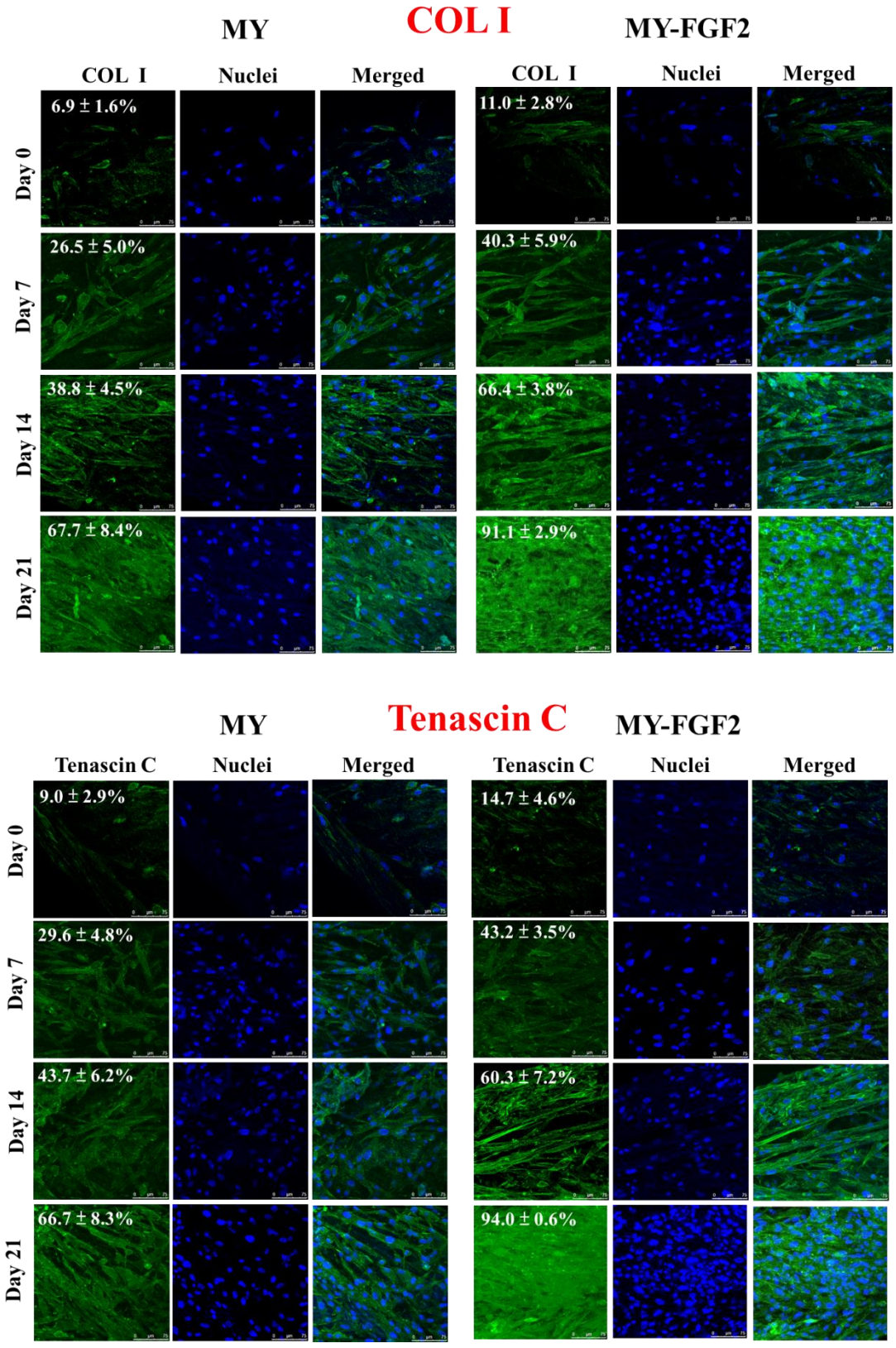

Figure 6. The confocal microscopy observation of rTFs cultured in MY or MY-FGF2 scaffolds up to 21 days after staining type I collagen (COL I) or tenascin C with FITC-tagged antibody (green) and cell nuclei with DAPI (blue) (bar = 75 μm). The numbers shown are semi-quantitative analysis of green fluorescence area percentages within each image.

3.3 In vitro studies: dynamic culture

As MY-FGF2 provides the best cues for tenogenic differentiation of rTFs, the MY-FGF2/rTFs was further dynamically cultured in vitro under cyclic tensile loading in a bioreactor. A previous study used 3, 6 or 9% cyclic loading on rabbit Achilles tendons at 0.25 Hz for 8 h/day to identify the optimal loading condition that can mimic the in vivo strain environments of tendons [47]. The results confirmed that a tendon without loading strain lost it structural integrity; 3% of cyclic tensile loading lead to moderate matrix deterioration and elevated expression levels of MMP-1, 3, and 12; loading at 9% caused massive rupture of collagen bundle. In contrast, 6% cyclic strain-loaded tendons displayed structural integrity and cellular function and thereby declaring the importance of mechanical stimulation in tendon regeneration. Considering this study, the cyclic loading in MY-FGF2 was proposed at 3 and 5% strain for dynamic culture, and static culture in the same bioreactor without mechanical loading (0% strain) was used as a reference for comparison. After dynamic culture, MY-FGF2/rTFs constructs were observed under SEM for cell adhesion and the morphology of adhered cells. Surprisingly, the density and morphology of cells in MY-FGF2 under dynamic culture was totally different from those under static culture. Each single yarn in MY-FGF2 scaffolds was covered up with a cell layer of rTFs, whose thickness increases with increasing strain value **(Figure 7A)**. The elongated orientation of rTFs under dynamic culture is also visible from the SEM images. The observation of higher cell density was supported form DNA content measurements, indicating proliferation rate of rTFs is positively correlated with the value strain up to 5% **(Figure 7B)**. For cell orientation, the cytoskeletal staining found the actin filament deposition is oriented along the fiber axis under dynamic culture, together with more stained nuclei (**Figure 7C)**. The highest cellular density as well as actin cytoskeleton expression at 5% strain underlines the importance of mechanical stimulation during cell growth.

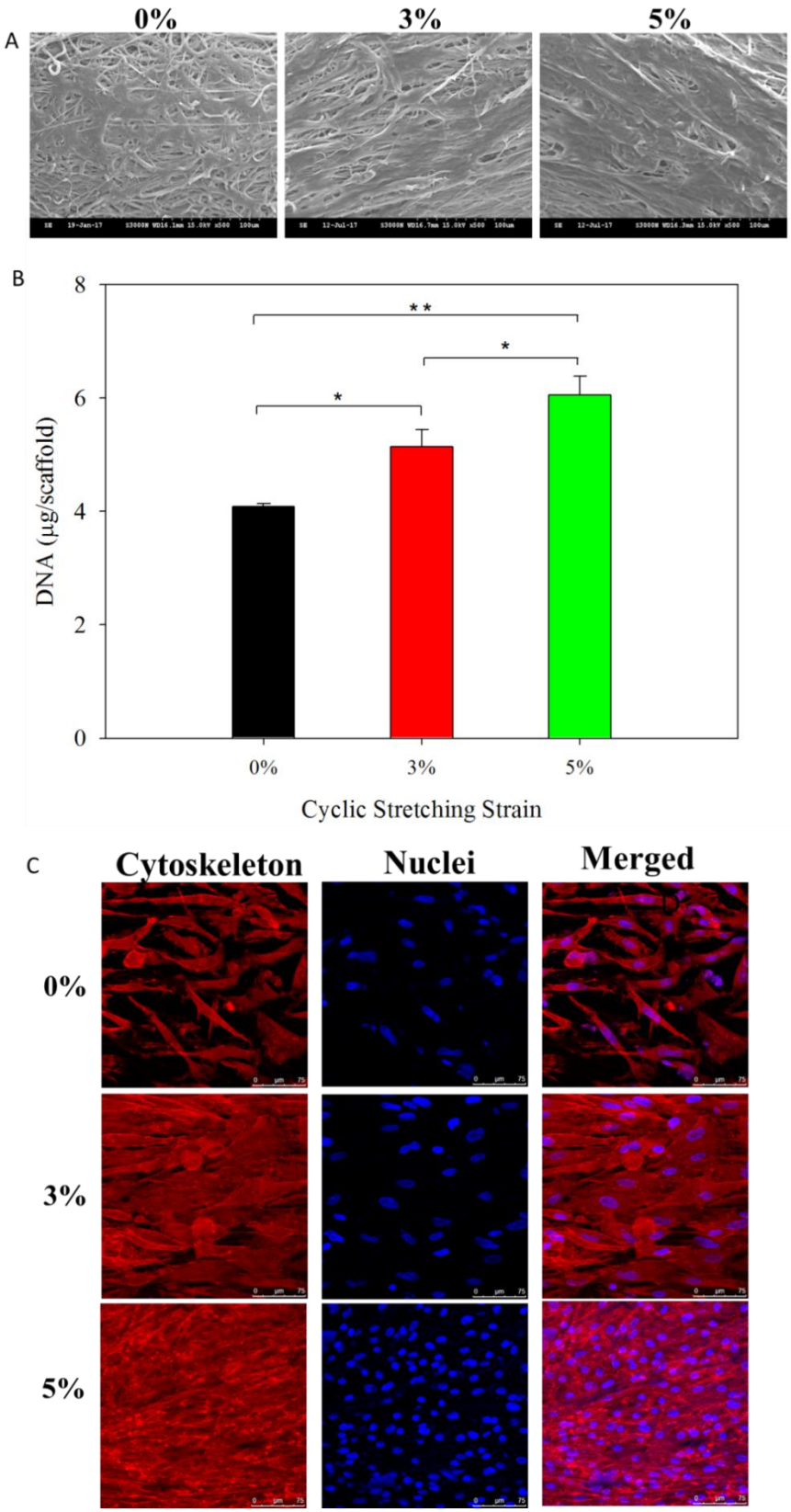

Figure 7. The cell morphology from SEM (A, bar = 100 μm), the cell proliferation from DNA contents (B), and the staining of actin filaments cytoskeleton (C, bar = 75 μm) after mechanical stimulation of MY-FGF2/rTFs by culture in a bioreactor for 7 days with 3 h stretching per day at 0.5 Hz frequency, and with 0, 3 or 5% strain. *$p < 0.05$, **$p < 0.01$.

For gene expression under dynamic culture, mechanical stimulation promotes the expression of COL I and tenascin C gene, with the relative mRNA levels influenced by the strain value **(Figure 8).** The expression of COL I is in the order 0% < 3% <5%, indicating mechanical stimulation promotes tenocyte maturation and synthesis of ECM [48]. Similar to COL I, the gene expression of tenascin C is also highly up-regulated from mechanical stimulation. A reverse trend was found for COL III and fibronectin. As stated before, COL III is an early gene expressed during the tendon regeneration process, where it will be converted into COL I as tendon matures [38]. Therefore, COL III expression is the highest at 0% strain and decreased with increasing cyclic stretching strain. The COL III gene expression drastically dropped at 5% stretching, implying mechanical stimulation can increase the tendon maturation rate. Fibronectin is an early expressing gene during the attachment and survival of the cells. During tendon repair, it will be expressed in large quantities throughout the growth period. The fibronectin gene expression of rTFs decreased significantly by cyclic tensile loading, which reveals the relevance of mechanical stimulation towards successful tendon regeneration [42]. Unlike gene expression patterns of other genes, biglycan exhibited similar mRNA levels irrespective of cyclic stretching stain at 0, 3 or 5%. The unchanged mRNA levels of biglycan thus confirms its gene expression was not affected by mechanical stimulation, as has been reported before [49].

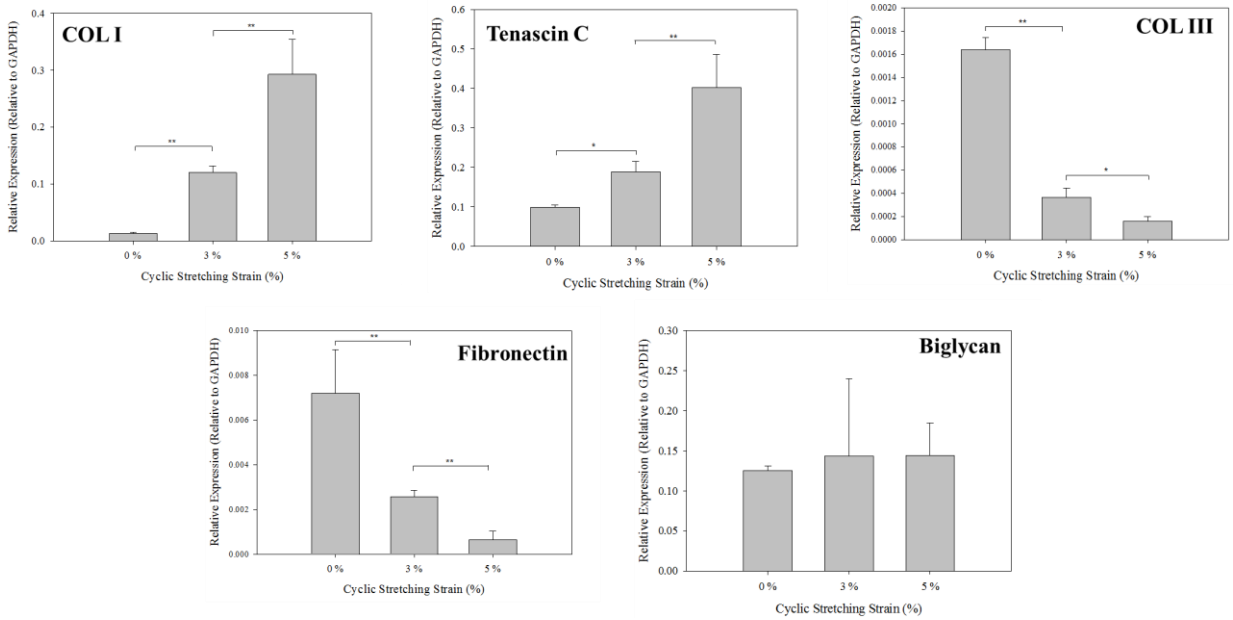

Figure 8. The gene expression analysis of type I collagen (COL I), tenascin C, type III collagen (COL III), fibronectin and biglycan from qRT-PCR after mechanical stimulation of MY-FGF2/rTFs by culture in a bioreactor for 7 days, with 3 h stretching per day at 0.5 Hz frequency, and with 0, 3 or 5% strain.

The effect of cyclic stretching on synthesis of key tendon marker proteins was examined through qualitative assessment of time-lapsed COLI and tenascin C fluorescence signal change during immunofluorescence (IF) staining. The deposition of both proteins is found to be increased with increasing strain value, as well as the density DAPI-stained nuclei **(Figure 9)**. The oriented deposition of FITC-labelled proteins re-affirms the influence from fiber orientation in the yarn bundles. Undoubtedly, the application of cyclic strain along the fiber axis provides pronounced effect on protein production and distribution, presumably from the directional mechanical stimulation during cell growth. The protein deposition therefore reaches the maximum under the highest cyclic stretching (5% strain). The semi-quantitative estimation of green fluorescence area in the confocal images is 48.7% for COL I and 34.2% for tenascin C at 0% strain. This value increases to 87.6% (3% strain) and 97.9% (5% strain) for COL I, and to 77% (3% strain) and 95.5% (5% strain) for tenascin C. These results are consistent with the fact that mechanical stimulation can enhance maturation of rTFs to enhance COL I and tenascin C production [50]. It is also consistent with the report that the direction during mechanical stimulation and fiber orientation of the scaffold could induce uniaxial cellular alignment by affecting cell morphology [51].

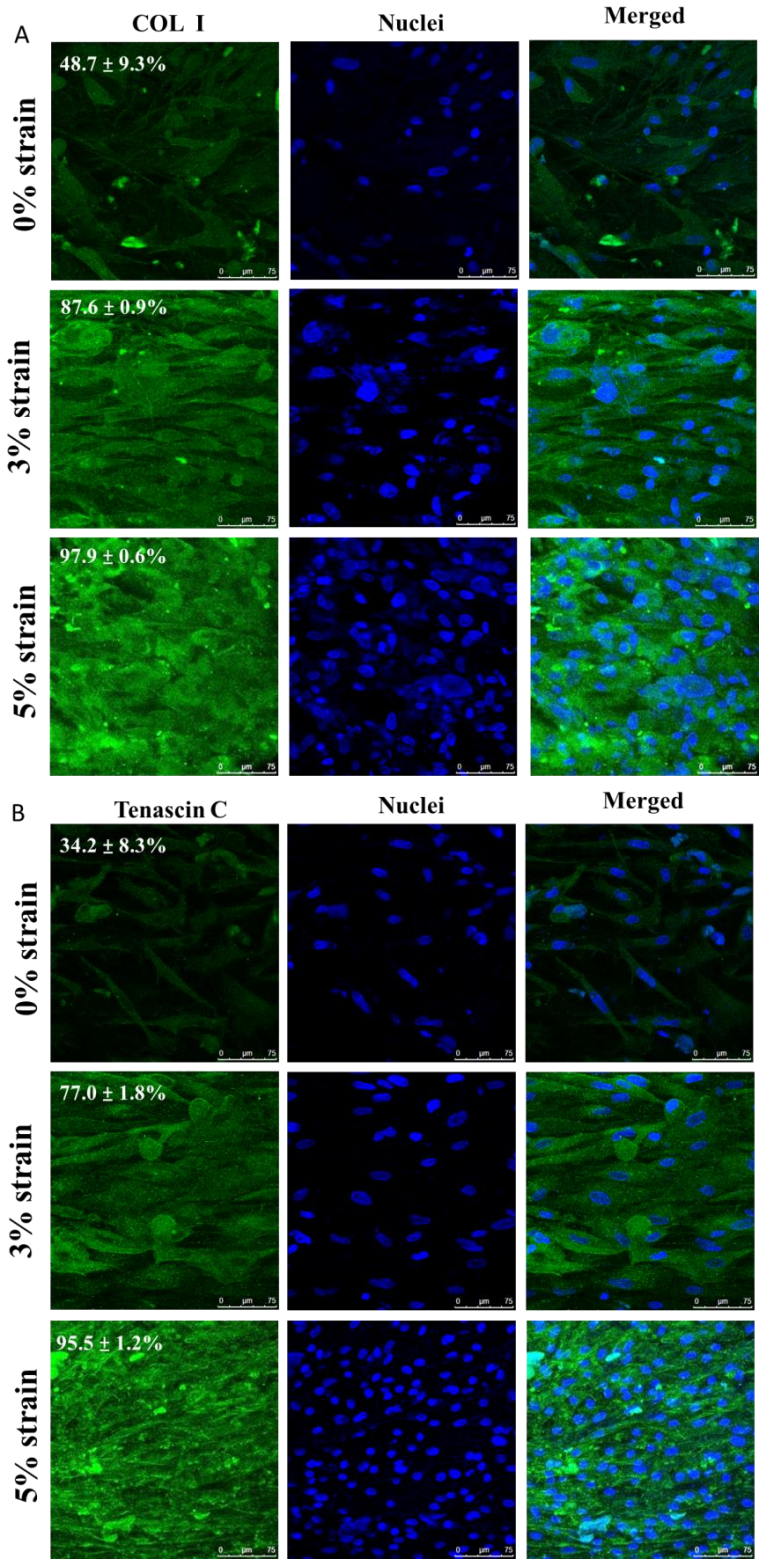

Figure 9. The immunofluorescence staining images of type I collagen (COL I) (A) and tenascin C (B). A MY-FGF2/rTFs construct was mechanically stimulated by culture in a bioreactor for 7 days, with 3 h stretching per day at 0.5 Hz frequency, and with 0, 3 or 5% strain. The protein was stained with FITC-tagged antibody (green) and cell nuclei were stained with DAPI (blue). The numbers shown are semi-quantitative analysis of green fluorescence area percentages within each image. Bar = 75 μm.

3.4 In vivo studies

The ability of a dynamic-cultured MY-FGF2/rTFs implant towards extensor digitorium tendon (EDT) regeneration was examined from the six-week harvested samples. During the experiment, a defect was created for an EDT and a cell-free (acellular) or a cell-seeded (cellular) MY-FGF2 scaffold was sutured to both ends of the created defect for repair (**Figure 10A**). The tendon disruption is clearly visible before implantation and the dimension of the MY-FGF2 scaffold was well-controlled to be matching the diameter and length of an EDT. Scaffolds were sutured to the terminals of each disruption end and the suturing was made intact through enlacing inside the tied terminals of MY-FGF2 scaffolds. Six-week after implantation, the scaffold appeared to be embedded in the native tendon through sutured terminals and gross view of neo-tendon confirmed the successful bridging of implanted scaffolds to the proximal and distal ends to initiate regeneration. There was no significant difference between the acellular and the cellular groups in appearance, but it can be observed that implant shape is not deformed 6 weeks from implantation. The mechanical stability of the scaffolds has been tested through physical pulling, using forceps. From the physical appearance it was confirmed that the suture-embedded yarn-based MY-FGF2 scaffold can be considered an alternative for the current knot problems of commercial microfibers used for tendon surgery [52].

To assess the tendon regeneration potential in vivo, H&E, Masson's trichrome and IHC staining of tendon specific marker protein COL I, Col III and tenascin C was performed (**Figure 10B)**. Compared with acellular samples, the H&E staining of cellular samples displayed highly organized tissue morphology. Abundant cells were found in the cellular sample in contrast to sporadic infiltrated cells in the acellular sample, where hematoxylin stains cell nuclei to purplish blue and eosin stains ECM and cytoplasm to pink, endorsing successful tissue regeneration [53]. In case of acellular samples, the intermittent voids and wavy appearance are due to the presence of fibrous environment without cellular proliferation. In further, the distribution of collagen fibers was analyzed through Masson's trichrome staining. As COL I is the most abundant component in the tendon tissue, the blue color from Masson's trichrome staining can be used to compare the collagen distribution in a neo-tendon tissue. The cellular scaffold obviously has a directional deposition of collagen fibers in dark blue, which is detected at negligible level in the acellular sample. The fiber-like parallel deposition confirms the initiation of collagen bundle formation in the implanted cellular construct. The appearance of minimum level of blue stain from the acellular sample

must be due to the migration of tendon cells from the proximal and distal ends of disrupted native tendons in rabbits.

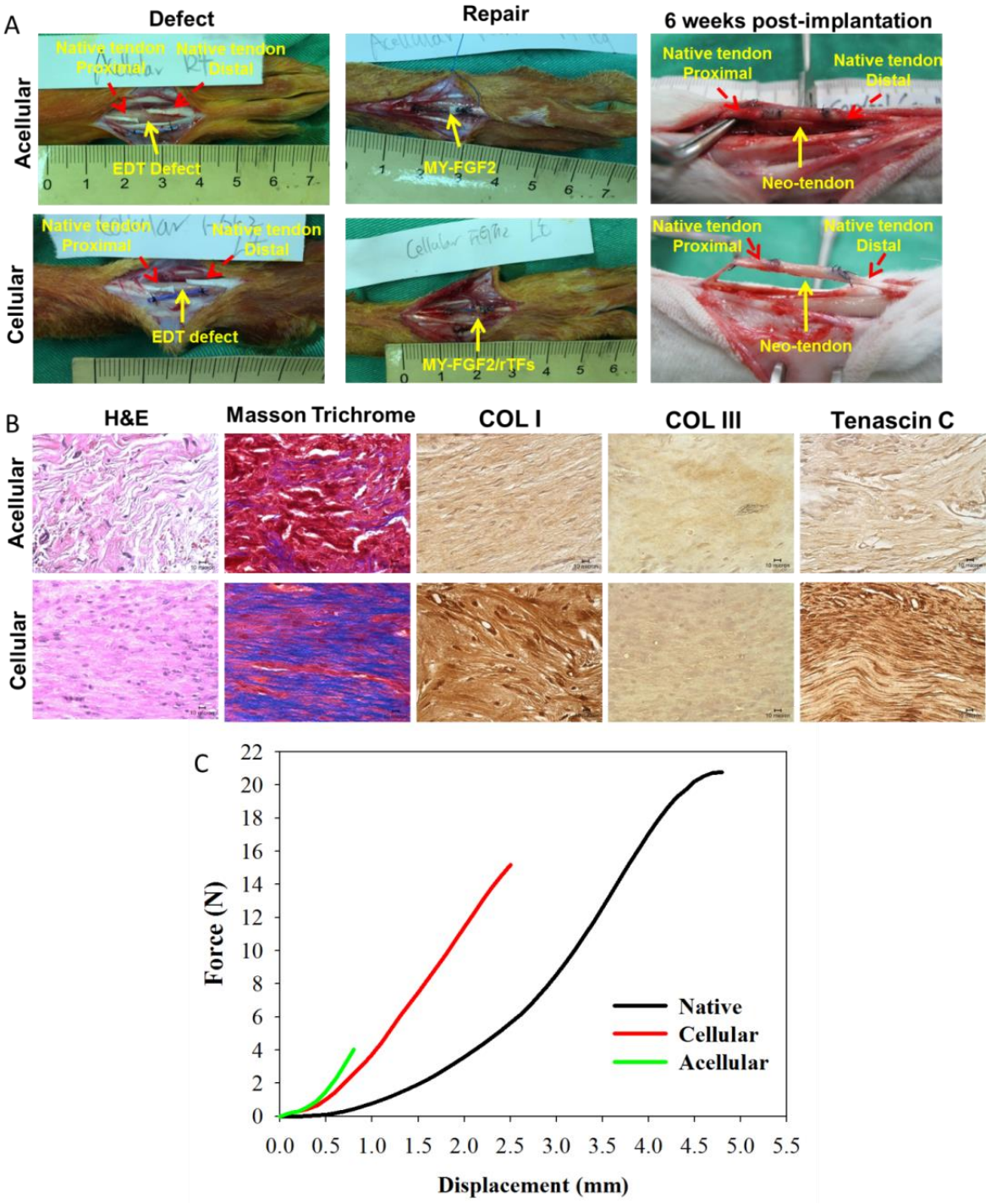

Figure 10. (A) The extensor digitorum tendon (EDT) defect was repaired with a MY-FGF2 scaffold (acellular) or a MY-FGF2/rTFs construct after 7-day in vitro cell culture at 5% strain (cellular), by suturing to distal and proximal ends of native tendon. The grafts were explanted 6-week after implantation. (B) The H&E stain, Masson's trichrome stain, immunohistochemical (IHC) analyses of tendon specific markers type I collagen (COL I), type III collagen (COL III) and tenascin C (bar = 10 μm). (C) The typical force-displacement

curves of native tendon, and cellular and acellular samples retrieved 6 weeks post-implantation, by tensile mechanical testing.

The IHC staining was further performed to identify the synthesis of tendon-specific proteins secreted by transplanted rTFs in the scaffold. As COL I is an important protein in the remodeling phase of the tendon, secreted by mature cells, it is more rational to examine the presence of COL I in the regenerating material to validate tendon growth. The dark brown deposition observed from COL I staining in the cellular sample indicates abundant presence of COL I, where acellular sample reveals only a light staining intensity (**Figure 10B**). Similar to the aligned deposition in observed from Masson's trichrome staining, COL I in cellular sample follows similar pattern and thus supports tendon regeneration. The dark brownish nodules appears in the cellular sample is due to the deposition of secreted COL I around cell surface, which can be verified from the nuclear staining nodules from H&E stain. As tenascin C is produced during the proliferation and re-construction phases during tendon healing, its secretion will be minimum at early stages and increase with time. That the staining intensity of tenascin C for the cellular sample is significantly higher than the acellular sample thus supports continuous tenogenic differentiation of rTFs in vivo. This can be correlated with the protein synthesis and gene expression levels observed in vitro. Both COL I and tenascin C deposit along the direction of bundle axis and thus entertain the elongated morphology of native tendons. COL III was verified further to analyze tendon formation, which is composed of shorter fibers and observed at the growth phase of tendon re-construction/regeneration. Being an early expressing protein, the secretion COL III will decrease with the maturation of cells and the growth of collagen fibers, and thus accounts for the light staining intensity observed (**Figure 10B**). Moreover, there was no significant difference is staining intensity between the cellular and acellular samples, and thus accounts for a mature neo-tendon tissue formed by the implanted MY-FGF2/rTFs construct. The down-regulated COL III staining intensity at 6-week implantation period compared with COL I points out the characteristic of enhanced tendon regeneration provided by MY-FGF2 after mechanical stimulation. Overall, the mechanically stimulated MY-FGF2 scaffolds pre-cultured with rTFs could be deemed as an ideal tissue engineering construct for tendon repair or replacement.

At the end of in vivo experiments, repaired tendons from the acellular and cellular groups were explanted and subject to biomechanical analysis using tensile testing. A native EDT was also retrieved and subject to the same test for comparison. As shown from the force (load) (N)-displacement (elongation) (mm) curves, both samples show characteristic tendon

mechanical behavior under tensile testing from the force-displacement curve, with an initial toe-region followed by a linear region till failure (**Figure 10C**). The mean value of stiffness, calculated from the slope of the linear region in the force-displacement curve for the cellular sample is 7.48 N/mm, which is similar to that of the acellular sample (6.98 N/mm) (**Table 2**). However, the maximum load and the maximum displacement at failure increase significantly from the acellular to the cellular sample. The mean values of maximum force increases from 6.22 N to 16.58 N, and the maximum displacement from 1.23 mm to 3.50 mm. This also results in 3.5-fold increase of stored energy for the cellular sample. Compared with a native tendon, only the cellular sample, but not the acellular one, shows similar stiffness, maximum displacement and maximum load force with no significant difference. Nonetheless, the stored energy of the cellular sample is still significantly less than that of a native tendon, representing only 45% of its mean value. This may arise from limited sample size and insufficient implantation time during in vivo studies. Although retrieved MY-FGF2 is with similar stiffness, only rTFs-seeded MY-FGF2 construct can generate a tendon structure with similar force and displacement with a native tendon tissue, presumably from production of tendon-specific proteins in the ECM of neo-tendon, as shown from the IHC images.

Table 2. The tensile mechanical properties of native tendons, and cellular and acellular samples retrieved 6 weeks post-implantation in a rabbit extensor digitorum tendon defect model (n = 3).

	Native	Cellular	Acellular
Maximum load (N)	20.26 ± 3.74	16.58 ± 3.05	6.22 ± 3.15 $^{\alpha,\beta}$
Maximum displacement (mm)	4.00 ± 1.13	3.50 ± 0.45	1.23 ± 0.84 $^{\alpha,\beta}$
Stiffness (N/mm)	7.20 ± 0.28	7.48 ± 1.18	6.98 ± 2.18
Energy (mJ)	32.93 ± 6.13	15.03 ± 5.10 $^{\alpha}$	4.24 ± 5.12 $^{\alpha,\beta}$

$^{\alpha}p < 0.05$ compared with native, $^{\beta}p < 0.05$ compared with cellular.

4. Conclusion

A suture-reinforced single yarn (SY) of PCL aligned fibers was prepared by collecting PCL fibrous structure with an extending commercial surgical suture. Three SY were successfully braided together to fabricate a multiple yarn (MY) scaffold with high flexibility, mechanical strength and fibrous surface topography. The fibers in the fibrous sheath can align in a twisting angle on top of the suture, which can be further surface grafted with heparin for

FGF2 binding to enable faster tendon regeneration. From spectroscopy and microscopy analysis, serial surface modification and surface grafting did not affect the yarn morphology. Thermogravimetric analysis and probing with FGF2-abtibody confirm the presence of heparin and FGF2 in the scaffold. In vitro studies with rTFs displayed higher cell proliferation in MY-FGF2 scaffold with high cell viability from Live/Dead staining and cell adhesion and proliferation in alignment with fiber orientation is observed from cytoskeletal staining. Up-regulated gene expression of tenogenic marker genes validates effective tendon regeneration using MY-FGF2 where enhanced synthesis of tenogenic marker proteins is also evident from immunofluorescence staining. When in vitro characterizations in static culture were compared with dynamic culture with 3% and 5% strain, MY-FGF2/rTFs mechanically stimulated at 5% strain displayed optimum cell proliferation rate, cytoskeletal expression, gene expression and protein synthesis. The regeneration efficiency of the optimized constructed fabricated in vitro was used for repair of tendon defect in rabbits with dissected EDT. The histological analysis and biomechanical analysis of the explanted samples six weeks after implantation not only reveal the regeneration capability of MY-FGF2/rTFs but also demonstrate its mechanical suitability to compete with an autologous tendon grafts. As of today, the commonly used non-degradable microfibrous scaffolds were lacking the ability to maintain a cell-friendly environment for tendon regeneration. In contrast, when fibrous scaffolds were proposed, none of them were capable to meet the extreme mechanical stability and flexibility demanded. In this context, the novel scaffold design proposed here is expected to have an impact on development of tendon grafts for clinical use.

Acknowledgements

We are thankful for financial supports from Chang Gung Memorial Hospital, Taiwan (CMRPD2J0111, CMRPD2J0112 and CMRPD2J0113) and the Ministry of Science and Technology, Taiwan (MOST 109-2314-B-182-013-MY3). K.T. Shalumon acknowledges the financial aid from the Ramalingaswami Fellowship, Department of Biotechnology, India. The technical support by the Microscopy Center, Chang Gung University and the Microscope Core Laboratory, Chang Gung Memorial Hospital, Linkou are acknowledged.

References

[1] M. Kjaer, Role of extracellular matrix in adaptation of tendon and skeletal muscle to mechanical loading, Physiological reviews 84 (2004) 649-698.

[2] C.T. Thorpe, H.R. Screen, Tendon Structure and Composition, Adv. Exp. Med. Biol. 920 (2016) 3-10.
[3] P.K. Nguyen, K. Baek, F. Deng, J.D. Criscione, R.S. Tuan, C.K. Kuo, 2.6.5 - Tendon Tissue-Engineering Scaffolds, in: W.R. Wagner, S.E. Sakiyama-Elbert, G. Zhang, M.J. Yaszemski (Eds.) Biomaterials Science (Fourth Edition), Academic Press2020, pp. 1351-1371.
[4] A. Sensini, G. Massafra, C. Gotti, A. Zucchelli, L. Cristofolini, Tissue Engineering for the Insertions of Tendons and Ligaments: An Overview of Electrospun Biomaterials and Structures, Frontiers in Bioengineering and Biotechnology 9 (2021).
[5] S. Ruiz-Alonso, M. Lafuente-Merchan, J. Ciriza, L. Saenz-del-Burgo, J.L. Pedraz, Tendon tissue engineering: Cells, growth factors, scaffolds and production techniques, J. Control. Release 333 (2021) 448-486.
[6] D.L. Butler, C. Gooch, K.R.C. Kinneberg, G.P. Boivin, M.T. Galloway, V.S. Nirmalanandhan, J.T. Shearn, N.A. Dyment, N. Juncosa-Melvin, The use of mesenchymal stem cells in collagen-based scaffolds for tissue-engineered repair of tendons, Nature Protocols 5 (2010) 849-863.
[7] S. Saber, A.Y. Zhang, S.H. Ki, D.P. Lindsey, R.L. Smith, J. Riboh, H. Pham, J. Chang, Flexor Tendon Tissue Engineering: Bioreactor Cyclic Strain Increases Construct Strength, Tissue Engineering Part A 16 (2010) 2085-2090.
[8] Z. Mao, B. Fan, X. Wang, X. Huang, J. Guan, Z. Sun, B. Xu, M. Yang, Z. Chen, D. Jiang, J. Yu, A Systematic Review of Tissue Engineering Scaffold in Tendon Bone Healing in vivo, Frontiers in Bioengineering and Biotechnology 9 (2021).
[9] J. Cai, X. Xie, D. Li, L.-R. Wang, J. Jiang, X.-m. Mo, J. Zhao, A novel knitted scaffold made of microfiber/nanofiber core-sheath yarns for tendon tissue engineering, Biomaterials science 8 (2020).
[10] Z. Zheng, J. Ran, W. Chen, Y. Hu, T. Zhu, X. Chen, Z. Yin, B.C. Heng, G. Feng, H. Le, C. Tang, J. Huang, Y. Chen, Y. Zhou, P. Dominique, W. Shen, H.-w. Ouyang, Alignment of collagen fiber in knitted silk scaffold for functional massive rotator cuff repair, Acta biomaterialia 51 (2017) 317-329.
[11] W. Zhang, Y. Yang, K. Zhang, Y. Li, G. Fang, Weft-knitted silk-poly(lactide-co-glycolide) mesh scaffold combined with collagen matrix and seeded with mesenchymal stem cells for rabbit Achilles tendon repair, Connective tissue research 56 (2015) 25-34.
[12] S. Wu, Y. Wang, P.N. Streubel, B. Duan, Living nanofiber yarn-based woven biotextiles for tendon tissue engineering using cell tri-culture and mechanical stimulation, Acta biomaterialia 62 (2017) 102-115.
[13] O. Hakimi, P.A. Mouthuy, N. Zargar, E. Lostis, M. Morrey, A. Carr, A layered electrospun and woven surgical scaffold to enhance endogenous tendon repair, Acta biomaterialia 26 (2015) 124-135.
[14] S. Wu, B. Duan, P. Liu, C. Zhang, X. Qin, J.T. Butcher, Fabrication of Aligned Nanofiber Polymer Yarn Networks for Anisotropic Soft Tissue Scaffolds, ACS Applied Materials & Interfaces 8 (2016) 16950-16960.
[15] S. Omeroglu, The effect of braiding parameters on the mechanical properties of braided ropes, Fibres and Textiles in Eastern Europe 14 (2006) 53-57.
[16] T.D.M.D. Rosenberg, Knee Ligaments. Structure, Function, Injury, and Repair, JBJS 73 (1991) 477.
[17] B.A. Smith, G.A. Livesay, S.L. Woo, Biology and biomechanics of the anterior cruciate ligament, Clinics in sports medicine 12 (1993) 637-670.
[18] W.-J. Li, Y. Jiang, R. Tuan, Chondrocyte Phenotype in Engineered Fibrous Matrix Is Regulated by Fiber Size, Tissue engineering (2006) 060802052515028.
[19] D.M. Kalaskar, F. Alshomer, Chapter 8 - Micro- and Nanotopographical Cues Guiding Biomaterial Host Response, in: S.J. Lee, J.J. Yoo, A. Atala (Eds.) In Situ Tissue Regeneration, Academic Press, Boston, 2016, pp. 137-163.
[20] C. Lee, H. Shin, I. Cho, Y.-M. Kang, I. Kim, K. Park, J.-w. Shin, Nanofiber alignment and direction of mechanical strain affect the ECM production of human ACL fibroblast, Biomaterials 26 (2005) 1261-1270.
[21] K. Spanoudes, D. Gaspar, A. Pandit, D.I. Zeugolis, The biophysical, biochemical, and biological toolbox for tenogenic phenotype maintenance in vitro, Trends Biotechnol. 32 (2014) 474-482.

[22] M. Hogan, K. Girish, R. James, G. Balian, S. Hurwitz, A.B. Chhabra, Growth differentiation factor-5 regulation of extracellular matrix gene expression in murine tendon fibroblasts, Journal of Tissue Engineering and Regenerative Medicine 5 (2011) 191-200.
[23] J.-P. Chen, W.-L. Lee, Collagen-grafted temperature-responsive nonwoven fabric for wound dressing, Appl. Surf. Sci. 255 (2008) 412-415.
[24] J. Zhang, J.H. Wang, Characterization of differential properties of rabbit tendon stem cells and tenocytes, BMC musculoskeletal disorders 11 (2010) 10.
[25] X. Zhang, W. Chang, P. Lee, Y. Wang, M. Yang, J. Li, S.G. Kumbar, X. Yu, Polymer-Ceramic Spiral Structured Scaffolds for Bone Tissue Engineering: Effect of Hydroxyapatite Composition on Human Fetal Osteoblasts, PloS one 9 (2014) e85871.
[26] Y.J. Kim, R.L. Sah, J.Y. Doong, A.J. Grodzinsky, Fluorometric assay of DNA in cartilage explants using Hoechst 33258, Analytical biochemistry 174 (1988) 168-176.
[27] J.P. Chen, M.J. Tsai, H.T. Liao, Incorporation of biphasic calcium phosphate microparticles in injectable thermoresponsive hydrogel modulates bone cell proliferation and differentiation, Colloids and surfaces. B, Biointerfaces 110 (2013) 120-129.
[28] C.H. Chen, D.L. Li, A.D. Chuang, B.S. Dash, J.P. Chen, Tension Stimulation of Tenocytes in Aligned Hyaluronic Acid/Platelet-Rich Plasma-Polycaprolactone Core-Sheath Nanofiber Membrane Scaffold for Tendon Tissue Engineering, Int. J. Mol. Sci. 22 (2021).
[29] W.-E. Teo, R. Gopal, R. Ramaseshan, K. Fujihara, S. Ramakrishna, A dynamic liquid support system for continuous electrospun yarn fabrication, Polymer 48 (2007) 3400-3405.
[30] U. Ali, Y. Zhou, X. Wang, T. Lin, Direct electrospinning of highly twisted, continuous nanofiber yarns, The Journal of The Textile Institute 103 (2012) 80-88.
[31] I.-K. Kang, O.H. Kwon, Y.M. Lee, Y.K. Sung, Preparation and surface characterization of functional group-grafted and heparin-immobilized polyurethanes by plasma glow discharge, Biomaterials 17 (1996) 841-847.
[32] S.-H. Chen, C.-H. Chen, K. Shalumon, J.-P. Chen, Preparation and characterization of antiadhesion barrier film from hyaluronic acid-grafted electrospun poly(caprolactone) nanofibrous membranes for prevention of flexor tendon postoperative peritendinous adhesion, International journal of nanomedicine 9 (2014) 4079-4092.
[33] O.A. Ibrahimi, F. Zhang, S.C. Lang Hrstka, M. Mohammadi, R.J. Linhardt, Kinetic model for FGF, FGFR, and proteoglycan signal transduction complex assembly, Biochemistry 43 (2004) 4724-4730.
[34] N.L. Leong, A. Arshi, N. Kabir, A. Nazemi, F.A. Petrigliano, B.M. Wu, D.R. McAllister, In vitro and in vivo evaluation of heparin mediated growth factor release from tissue-engineered constructs for anterior cruciate ligament reconstruction, J. Orthop. Res. 33 (2015) 229-236.
[35] L. Nieto, Á. Canales, I.S. Fernández, E. Santillana, R. González-Corrochano, M. Redondo-Horcajo, F.J. Cañada, P. Nieto, M. Martín-Lomas, G. Giménez-Gallego, J. Jiménez-Barbero, Heparin Modulates the Mitogenic Activity of Fibroblast Growth Factor by Inducing Dimerization of its Receptor. A 3D View by Using NMR, Chembiochem 14 (2013) 1732-1744.
[36] J. Bojsen-Møller, S.P. Magnusson, Mechanical properties, physiological behavior, and function of aponeurosis and tendon, Journal of Applied Physiology 126 (2019) 1800-1807.
[37] B.P. Chan, K.M. Chan, N. Maffulli, S. Webb, K.K. Lee, Effect of basic fibroblast growth factor. An in vitro study of tendon healing, Clinical orthopaedics and related research (1997) 239-247.
[38] I.R. Sigal, D.A. Grande, D.M. Dines, J. Dines, M. Drakos, Biologic and Tissue Engineering Strategies for Tendon Repair, Regenerative Engineering and Translational Medicine 2 (2016) 107-125.
[39] C.H. Jo, H.J. Lim, K.S. Yoon, Characterization of Tendon-Specific Markers in Various Human Tissues, Tenocytes and Mesenchymal Stem Cells, Tissue engineering and regenerative medicine 16 (2019) 151-159.
[40] W. Wang, J. He, B. Feng, Z. Zhang, W. Zhang, G. Zhou, Y. Cao, W. Fu, W. Liu, Aligned nanofibers direct human dermal fibroblasts to tenogenic phenotype in vitro and enhance tendon regeneration in vivo, Nanomedicine (London, England) 11 (2016) 1055-1072.

[41] J. Lu, L. Jiang, Y. Chen, K. Lyu, B. Zhu, Y. Li, X. Liu, X. Liu, L. Long, X. Wang, H. Xu, D. Wang, S. Li, The Functions and Mechanisms of Basic Fibroblast Growth Factor in Tendon Repair, Front. Physiol. 13 (2022) 852795.
[42] S. Sahoo, S.L. Toh, J.C. Goh, A bFGF-releasing silk/PLGA-based biohybrid scaffold for ligament/tendon tissue engineering using mesenchymal progenitor cells, Biomaterials 31 (2010) 2990-2998.
[43] J.R. Venugopal, S. Zhang Y Fau - Ramakrishna, S. Ramakrishna, In vitro culture of human dermal fibroblasts on electrospun polycaprolactone collagen nanofibrous membrane.
[44] R.A. Bagchi, J. Lin, R. Wang, M.P. Czubryt, Regulation of fibronectin gene expression in cardiac fibroblasts by scleraxis, Cell Tissue Res 366 (2016) 381-391.
[45] L.M. Dourte, L. Pathmanathan, M.J. Mienaltowski, A.F. Jawad, D.E. Birk, L.J. Soslowsky, Mechanical, compositional, and structural properties of the mouse patellar tendon with changes in biglycan gene expression, J. Orthop. Res. 31 (2013) 1430-1437.
[46] K.T. Shalumon, H.-T. Liao, C.-Y. Kuo, C.-B. Wong, C.-J. Li, M. P.A, J.-P. Chen, Rational design of gelatin/nanohydroxyapatite cryogel scaffolds for bone regeneration by introducing chemical and physical cues to enhance osteogenesis of bone marrow mesenchymal stem cells, Materials Science and Engineering: C 104 (2019) 109855.
[47] T. Wang, Z. Lin, R.E. Day, B. Gardiner, E. Landao-Bassonga, J. Rubenson, T.B. Kirk, D.W. Smith, D.G. Lloyd, G. Hardisty, A. Wang, Q. Zheng, M.H. Zheng, Programmable mechanical stimulation influences tendon homeostasis in a bioreactor system, Biotechnology and bioengineering 110 (2013) 1495-1507.
[48] N. Sawaguchi, T. Majima, T. Funakoshi, K. Shimode, K. Harada, A. Minami, S.-I. Nishimura, Effect of cyclic three-dimensional strain on cell proliferation and collagen synthesis of fibroblast-seeded chitosan-hyaluronan hybrid polymer fiber, Journal of Orthopaedic Science 15 (2010) 569-577.
[49] C. Popov, M. Burggraf, L. Kreja, A. Ignatius, M. Schieker, D. Docheva, Mechanical stimulation of human tendon stem/progenitor cells results in upregulation of matrix proteins, integrins and MMPs, and activation of p38 and ERK1/2 kinases, BMC Mol. Biol. 16 (2015) 6.
[50] Y. Xu, S. Dong, Q. Zhou, X. Mo, L. Song, T. Hou, J. Wu, S. Li, Y. Li, P. Li, Y. Gan, J. Xu, The effect of mechanical stimulation on the maturation of TDSCs-poly(L-lactide-co-e-caprolactone)/collagen scaffold constructs for tendon tissue engineering, Biomaterials 35 (2014) 2760-2772.
[51] Savio L.-Y. Woo, Richard E. Debski, Jennifer Zeminski, Steven D. Abramowitch, M. Serena S. Chan Saw, and, J.A. Fenwick, Injury and Repair of Ligaments and Tendons, Annual review of biomedical engineering 2 (2000) 83-118.
[52] S. Rawson, S. Cartmell, J. Wong, Suture techniques for tendon repair; a comparative review, Muscles, ligaments and tendons journal 3 (2013) 220-228.
[53] D.W. Youngstrom, J.G. Barrett, R.R. Jose, D.L. Kaplan, Functional characterization of detergent-decellularized equine tendon extracellular matrix for tissue engineering applications, PLoS One 8 (2013) e64151.

Declaration of interests

☐The authors declare that they have no known competing financial interests or personal relationships that could have appeared to influence the work reported in this paper.

☒The authors declare the following financial interests/personal relationships which may be considered as potential competing interests:

Jyh-Ping Chen reports financial support was provided by Chang Gung Memorial Hospital Linkou. Jyh-Ping Chen reports financial support was provided by Ministry of Science and Technology.